Stony Brook University

Funneling electron beams from gallium arsenide photocathodes

A Dissertation Presented

by

Omer Habib Rahman

to

The Graduate School

in Partial Fulfillment of the Requirements

for the Degree of

Doctor of Philosophy

in

Physics

Stony Brook University

August 2016

Stony Brook University

The Graduate School

Omer Habib Rahman

We, the dissertation committee for the above candidate for the

Doctor of Philosophy degree, hereby recommend

acceptance of this dissertation

Ilan Ben-Zvi - Dissertation Advisor
Professor, Department of Physics and Astronomy

Abhay Deshpande - Chairperson of Defense
Professor, Department of Physics and Astronomy

Dmitri Kharzeev - Committee Member
Professor, Department of Physics and Astronomy

Dejan Trbojevic - External Member
Senior Physicist,Brookhaven National Laboratory

This dissertation is accepted by the Graduate School

Charles Taber
Dean of the Graduate School

Abstract of the Dissertation

Funneling electron beams from gallium arsenide photocathodes

by

Omer Habib Rahman

Doctor of Philosophy

in

Physics

Stony Brook University

2016

Gallium Arsenide (GaAs) is the most widely used source of polarized electrons around the world. Electrons are extracted from a GaAs surface, terminated by a cesium-oxygen layer. The electrons are accelerated to form a beam by a DC electric field. This beam can ionize residual gas in the chamber, and the DC field accelerates the resulting ions into the cathode surface, damaging the Cesium-Oxygen layer. This process, called Ion Back Bombardment, is the dominant mechanism for limiting photocathode lifetime. As a result, high average current operation yields charge lifetimes too low to be used in a collider design.

One idea to extend the charge lifetime is to funnel the beams from multiple cathodes using a rotating magnetic field − if operation of one cathode does not affect the operation of another cathode in the same chamber, then the source's lifetime can be extended by simply adding more cathodes. This dissertation presents the design, construction and commissioning of a unique electron gun capable of operating twenty cathodes. Results of funneling two

electron beams with a rotating magnetic field are also presented. For average currents at 175 nA and 350 nA, the charge lifetimes for individual cathodes and two-cathode operation were measured, showing that the charge lifetime for two beam funneling is the sum of the individual ion back bombardment charge lifetimes. The addition of charge lifetime implies that beam funneling can be used to increase charge lifetime by an order of magnitude.

Contents

List of Figures

List of Tables

Chapter 1

Introduction

The purpose of this dissertation is to show that **if ion back bombardment is the dominant mechanism for photocathode lifetime decay, the charge lifetime of two cathode combined operation in low repetition rate is the sum of their individual charge lifetimes for the same average current**.

Polarized electron sources are of prime importance in the field of high energy and nuclear physics, particularly in fixed target parity violation experiments, understanding the spin structure of the nucleons etc. The very first polarized electron sources were based on spin exchange in atomic systems such as photo-ionization of spin polarized atoms[6], photo-ionization of unpolarized atoms by circularly polarized light (Fano effect)[7] etc. The early 1970's saw the dawn of the first 'designer' photocathode of the III-V family, Gallium Arsenide (GaAs). The possibility of extracting polarized electrons from GaAs was predicted based on the analysis of the well-defined band structure of the material [8]. Within the next decade, generation of spin polarized electrons from GaAs using a circularly polarized light was demonstrated by multiple research groups [9] [10]. The fact that the electron density of a crystal is much higher compared to the gas phase source, these photocathodes were of great interest towards a high current polarized electron source. Another big advantage of using GaAs as a source is that it can achieve 'Negative Electron Affinity' or NEA. The NEA condition means that the energy of the electron just outside the material surface (vacuum) is lower than the energy at the conduction band minimum. Therefore once the electrons are excited from the valence band to the conduction band, given the electrons can make it to the material surface, NEA makes it energetically possible to escape from the crystal surface into vacuum. In order to achieve the NEA condition, a very thin layer of Cesium and Oxygen is deposited on the surface of the photocathode. This surface treatment, often referred to as 'activation', can increase the eletron emission ten a few orders of magnitude to untreated GaAs [11]. Quantum efficiency, which is defined as the number of electrons emitted from the material per photon, can be 5% for photons that has energy close to the band gap and even higher for more energetic photons. In chapter 2, the properties of GaAs and photoemission process are discussed..

In order to extract polarized electrons from GaAs, the crystal is illuminated by a circularly polarized light with photon energy close to the band gap energy [10]. The photoexcitation of the electron from the valence band to the conduction band is a spin selective process. However, the degeneracy of the heavy hole and light hole valence bands in bulk GaAs limits the polar-

ization of electrons to 50% [3]. In practical applications, the polarization is about 40% due to spin depolarizing scattering mechanisms in the crystal [3]. In order to achieve higher polarization, the heavy hole-light hole degeneracy is broken by introducing a compressive biaxial strain which breaks the crystal symmetry. This type of GaAs is commonly referred to as Strained Superlattice GaAs. The ideal polarization from strained superlattice GaAs should be 100%. The polarization from optimized strained GaAs was measured to be 86% [12]. KEK/Nagoya university and SLAC has measured polarization from strained superlattice GaAs to be better than 80% [13].

Besides the degree of polarization, the most commonly used figure of merit for a polarized electron source is charge lifetime [14]. The charge lifetime of a cathode is defined as the amount of charge extracted from the photocathode before the quantum efficiency drops to $1/e$ of its initial value. Charge lifetime of a source is highly dependent on the static and dynamic vacuum of the system, beam loss during transport, the field emission in the DC gap, the quality of the photocathode activation including the size of the active area, the quality of the laser spot etc. In other words, the charge lifetime for different guns with different geometry while using the same material could vary vastly depending on any of the above mentioned parameters. Recently, the idea of fluence lifetime, defined as charge extracted per unit area, has come to prominence as the ultimate figure of merit for a DC photogun [15]. However, the fluence lifetime is also dependent on the many aforementioned conditions in the gun and is only repeatable in a gun given that the conditions remain the same.

There are multiple technical challenges in using GaAs for accelerator purposes. The monolayer of Cs-O on the GaAs surface is highly sensitive to vacuum and requires pressure below 10^{-11} Torr for preparation and operation [16]. Even at extremely good vacuum, chemically active gases like water, O_2 and CO_2 can contribute to the chemical poisoning of the cathode over a long period of time[17]. During operation, the dominant mechanism for cathode lifetime degradation is ion back bombardment. Mainz and Bates were the first groups to observe ion back bombardment damage on the illuminated side of a photocathode during beam operation [18]. In this process, the electron beam ionizes the gas molecules present in the gun chamber. These ions then get accelerated towards the cathode due to the electric field and eventually hit the cathode near its electrostatic center. Depending on the mass and energy of the ions, they can damage the activated surface of the cathode by sputtering the Cs-Oxygen layer, creating visible physical damage on the crystal etc. Heat cleaning and reactivation of the sample can fix some of the damages, however

prolonged ion back bombardment damage would eventually make a crystal unusable for beam operations [17]. Ion back bombardment is directly proportional to the average current extracted from the cathode and the pressure of the system[14]. Therefore high average current operations from GaAs limits the lifetime of the cathode greatly which makes high average current polarized sources very challenging.

In order to explore a new regime of QCD, a "Electron-Ion Collider (EIC)" has been proposed [19]. By virtue of high energy and high luminosity collisions at the proposed EIC, decisive measurements about various unanswered topics in QCD– including the proton spin, quark hadronization, motion of quarks and gluons in fast moving proton etc.– can be made [20]. Two separate designs for a EIC has been proposed in the US– eRHIC at Brookhaven National Lab and MEIC at Jefferson Lab. eRHIC requires a polarized electron source with 50 mA of average current [21]. Experiments in Jlab has shown that a single cathode DC polarized electron gun can be operated at 4 mA of average current for 5.5 hours [22]. This operational lifetime is expected to be even lower for an average current of 50 mA. So a practical design towards a high current polarized electron source is absolutely necessary for eRHIC. In the recent past, there has been two separate approaches to solve the problem of low charge lifetime at high average current. MIT- Bates has been developing a DC polarized gun where the cathode is much larger compared to conventional single cathode guns [23]. The core concept of this gun is to extract electrons in the form of a donut shape from the cathode, avoiding the center which would be damaged by ion back bombardment. At Brookhaven National Lab, the idea of combining multiple electron beams from multiple sources is being investigated [24]. The idea of funneling beams was first explored in the 1970's[25]. Stovall et al. [26] have studied funneling two ion beams at Los Alamos National Laboratory. However, the funneling concept has never been implemented for polarized electrons. In this approach, beams from multiple cathodes could be combined using a rotating magnetic field to extend the charge lifetime of the source, given that individual cathode operation is independent and ion back bombardment is the dominant mechanism for lifetime decay. If the charge lifetimes of two cathodes can be added to obtain double the charge lifetime, this idea can be extended to more than two cathodes to achieve the desired average current and charge lifetime. Section 4.1 describes the beam combination scheme to extend charge lifetime.

In this dissertation, we demonstrate that charge lifetimes from two bulk GaAs photocathodes can be added by combining the beam while operating

them in the same vicinity. lifetime measurements for average currents of 175 nA and 350 nA was done using two cathodes. First we measured the single cathode charge lifetime by driving one cathode at a time for one set of average current. Then the beam combination at 1 Hz repetition rate was performed for the same average current to see if the charge lifetime of the source gets doubled when the number of operating cathodes is doubled. If charge lifetimes can be added under suitable conditions in a polarized guns, the problem of low charge lifetime from a single photocathode for mA range operation can be solved by adding multiple cathodes. For this measurements, we used a unique electron gun with the capability of accommodating and operating multiple cathodes. The detail designs of the cathode preparation chamber and the gun are discussed in detail in chapter 3 . The experimental procedure, results and discussion are presented in chapter 4. The scope of the results and future work is discussed in chapter 5.

Chapter 2

GaAs photocathodes: Properties and operation in DC guns

Polarized electrons are used in high energy physics, nuclear physics and surface sciences as a probe to investigate the property of certain materials. Since the discovery of GaAs a possible source of polarized electrons in the 1970's, the material have been studied and used in practical accelerators all around the world. Currently CEBAF [27] at Jefferson Lab and MAMI at Mainz [28] , are the two facilities that deliver polarized electron beams for fixed target experiments. Both facilities use strained superlattice GaAs as photocathode to deliver electron beams with polarization higher than 80%. The future electron-ion collider project will require a polarized electron source with 50 mA average current [21] which is much higher than the current state of the art 4 mA average current [22]. Bulk GaAs was used for the experiments performed for this dissertation and this chapter discusses properties of bulk GaAs and challenges involved in operating a DC electron gun with bulk GaAs as the photocathode.

2.1 GaAs Photocathodes

III-V semiconductors, GaAs in particular, are the first class of materials to be designed to be used as a photoemitter of polarized electrons. [11]. These semiconductors are direct bandgap semiconductors with high photon absorption rate, fast time response and long diffusion length [29]. They can also achieve NEA (Negative Electron Affinity), where the conduction band minimum in the bulk of the material is higher than the potential barrier at the surface, which increases the rate of electrons emitted per photon compared to other conventional sources of electrons [30].

2.1.1 Crystal Structure

GaAs crystal has a zincblende crystal symmetry [2]. The lattice is an interpenetrating face-centered cube such that each atom is surrounded by four nearest neighbors positioned as the vertices of a regular tetrahedron. Two electrons of opposite spin create the nearest neighbor bonds [31]. The crystal structure of GaAs is shown in figure 2.1 and different crystal properties of GaAs are listed in table 2.1. The (100) plane is used as the photoemitting surface due to its having the highest quantum efficiency. GaAs cleaves the easiest at the (110) plane. During high temperature cleaning, the (100) plane can transform into (110) plane [32], so maintaining crystal temperature during heat cleaning is crucial.

Gallium	Z = 31, Family:IIIA
Arsenic	Z = 33, Family:VA
Lattice constant	a = 5.65 A^0
Nearest neighbor distance	$r_0 = \sqrt{3}a/4 = 2.45A^0$
Angle between bonds	109.47^o
Density	5.32 g/cm^3
Specific heat capacity	0.327 J/g-K
Thermal conductivity	0.55 W/cm.K
Band gap at 300K	1.42 eV

Table 2.1: Properties of GaAs

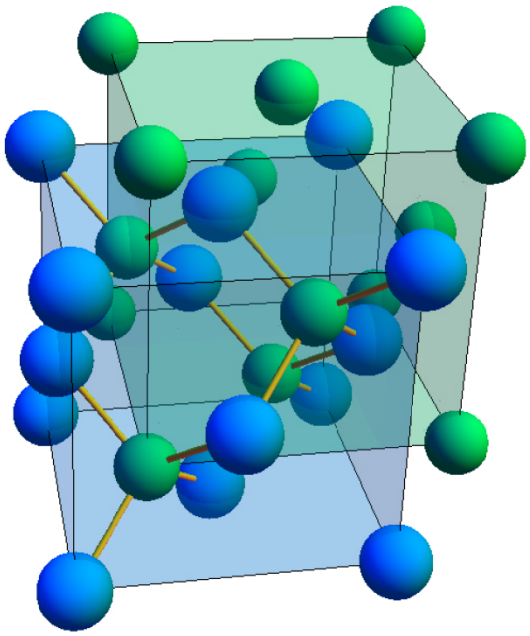

Figure 2.1: GaAs lattice structure showing the inter-penetrating face-center cubic structure [1]

2.1.2 Band structure

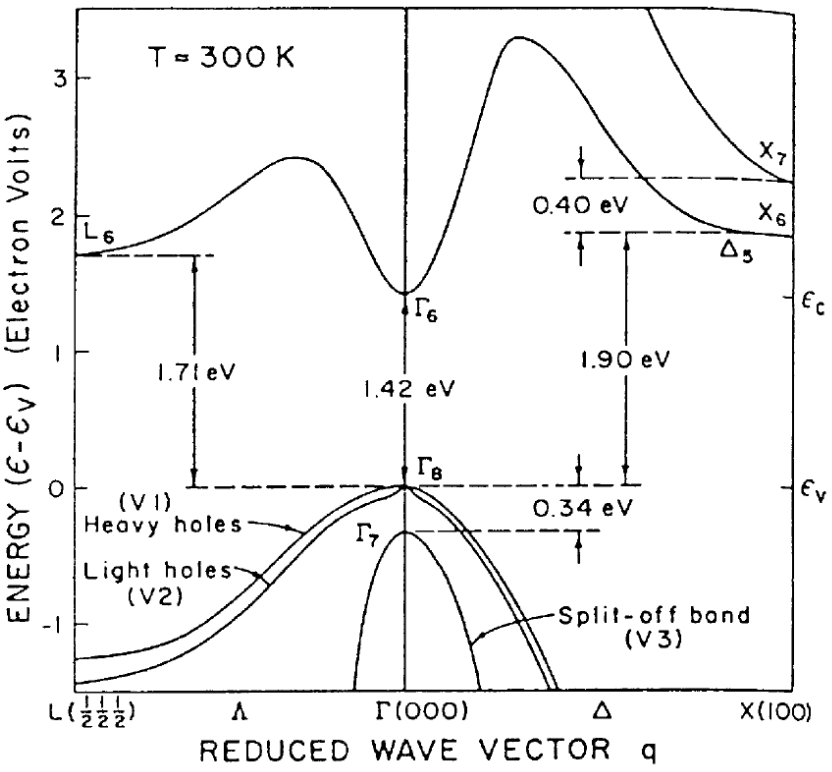

Figure 2.2: Band structure of bulk GaAs [2]

The band structure of a material is the energy-momentum relationship for an electron in the material [33]. This relationship is obtained by solving Schroedinger's equation for a periodic potential with the same periodicity as the lattice. The energy level solutions generally include a set of bands with higher energy values and a set of bands with lower energy values. The higher energy value bands are called the conduction bands and the lower energy value bands are called valence bands. The energy region between the conduction band and the valence bands is called the forbidden region, i.e. no electron can have energy states that lies in the forbidden region. The difference of energy between the conduction band minimum and the valence band maximum is called the band gap. For metals, this gap is very small or in some cases non-existent. For semiconductors, this gap is generally between 1 to 5 eV at room temperature [33]. If the conduction band minimum and the valence band maximum occurs at the same wave vector $\vec{k}$, the material is a 'direct band gap' semiconductor.

The band structure of bulk GaAs is shown in figure 2.2. It is a direct band gap semiconductor with 1.42 eV band gap at the Γ point ($\vec{k} = 0$). The upper valence bands have a L =1 angular momentum symmetry resulting in a three-fold degeneracy when spin is not taken into account. With spin included, the spin-orbit interaction breaks the symmetry resulting the creation of a 'Split-off Band' which lies 0.34 eV at T = 300 K^o below the doubly degenerate 'Heavy Hole (HH)' and 'Light Hole (HH)' bands at the Γ point. The conduction band minimum has only spin degeneracy and happens at the Γ point as well.

2.2 Photoemission from GaAs and polarized electrons

2.2.1 Spicer's three step model

The photoemission process from semiconductors was first explained by Spicer [34] using a simple three step model. Until then, photoemission was considered to be a surface effect[35]. Spicer considered the photoemission to be a bulk process consisting of three steps:

- The photo-excitation of electrons from the valence band to the conduction band.
- The transport of electrons from the bulk of the material to the surface.
- The emission of electrons from the surface to the vacuum.

Figure 2.3 shows the three steps involved in a photoemission process. In the first step, electrons in the valence band get excited to the conduction band by absorbing incoming photons with energy above the band gap. The optical absorption length plays a key role in how many electrons can be excited to the conduction band for a specific intensity of the light. A high optical absorption length would mean that electrons deep in the material can be excited to the conduction band. Amongst direct band gap semiconductors, GaAs has a high optical absorption coefficients [36] and therefore is a good candidate to be used as a photoemitter.

During the second step, the excited electrons on the conduction band approach the surface from the bulk of the material. While approaching the

surface, the electrons go through different scattering processes and thermalize to the bottom of the conduction band. Depending on what the dominant scattering mechanism is, the electrons will either have enough energy to stay at the conduction band while they reach the surface or will lose enough energy in scattering processes while approaching the surface to drop down to valence band and not be able to leave the surface. For example, if electron-electron scattering is the dominant mechanism, the excited electrons will lose its energy shortly after being excited to the conduction band and get back to valence band. This process is dominant in metals and solely responsible for the low quantum efficiency for metal photocathodes compared to semiconductor photocathodes. In semiconductors, electron-phonon scattering is the dominant mechanism which is not as lossy compared to electron-electron scattering. Scattering lengths in semiconductors are much higher and the excited electrons in the bulk have a high probability to reach the surface for emission.

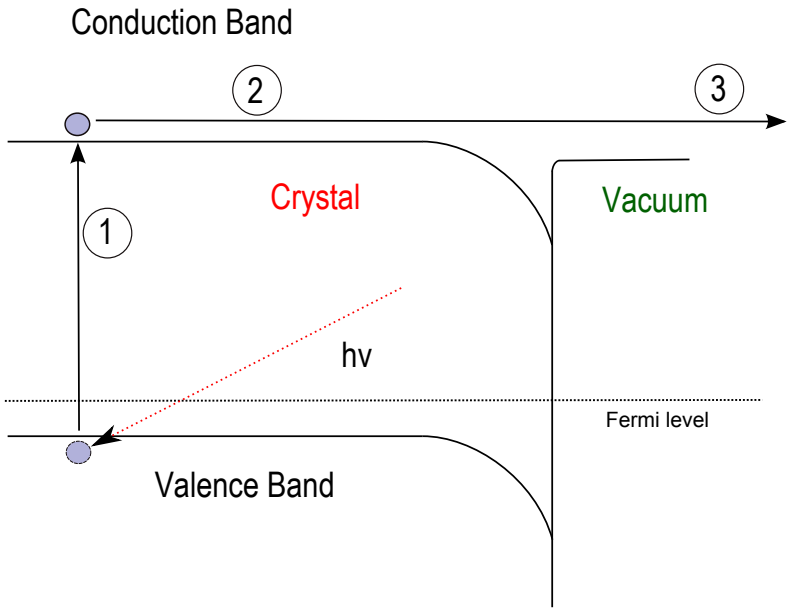

Figure 2.3: Spicer's three step photoemission process. 1- Photoexcitation of electron from valence to conduction band. 2- Electron transport from bulk to surface. 3- Emission of electron from surface to vacuum.

The third and final step of photoemission is the emission of electrons from the surface of the material to vacuum. The probability of emission of an electron from the surface to vacuum is dependent on surface characteristics of the material. For GaAs, the surface can be treated such that the potential difference between vacuum level and conduction band minimum is negative. This condition is called Negative Electron Affinity and is discussed in detail in section 2.2.2.

Using this model, the quantum efficiency of a photocathode was calculated to be [29],

$$QE = \frac{(\frac{\alpha_{PE}}{\alpha})P_E}{1 + \frac{l_a}{L}} \tag{2.1}$$

Where:
α_{PE} = Absorption coefficient for electrons excited above the vacuum level.
α = Absorption coefficient for the semiconductor.
P_E = Escape probability of an electron reaching the surface.
$l_a = \frac{1}{\alpha}$ = Photon absorption length for the material.
L = Electron diffusion length.

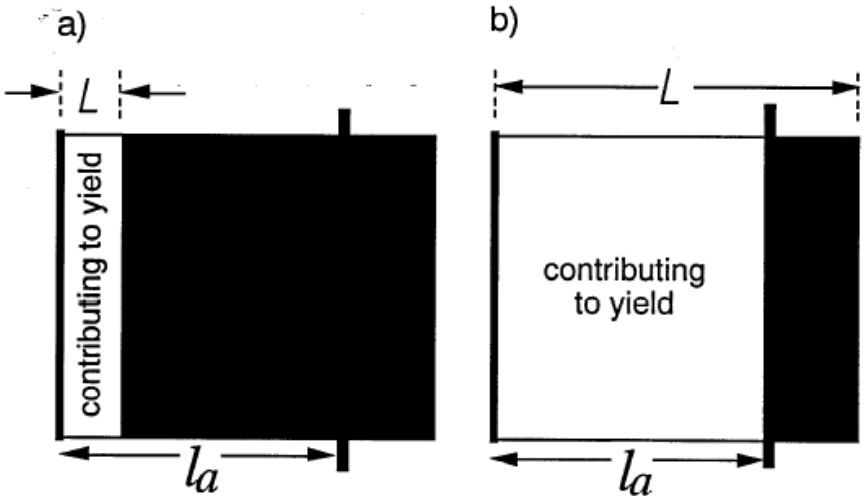

Figure 2.4: The dependency between optical absorption length (l_a) and electron diffusion length (L)

From equation 2.1, the ratio of l_a and L needs to be close to unity in order to maximize the quantum efficiency. If electrons diffusion length is too small

or the absorption length is too long compared to the diffusion length, electron emission will decrease. Figure 2.4 shows the dependency between the optical absorption length and the electron diffusion length.

The ratio of α_{PE} to α gives the fraction of electrons that are excited above the vacuum level. If vacuum level could be lowered, this ratio will increase and therefore photoemission rate will increase. For negative electron affinity photocathodes, this ratio can be close to unity.

2.2.2 Negative electron affinity

The third step of Spicer's model is the emission of electrons that has reached the surface of the material after being excited from the valence band to the conduction band via photoexcitation.The probability of electron emission from the surface to vacuum is maximized by achieving Negative Electron Affinity on the surface. This is done by using p doping to create a band bending region and then depositing monolayer quantities of Cs and an oxidant on the surface to create a dipole layer.

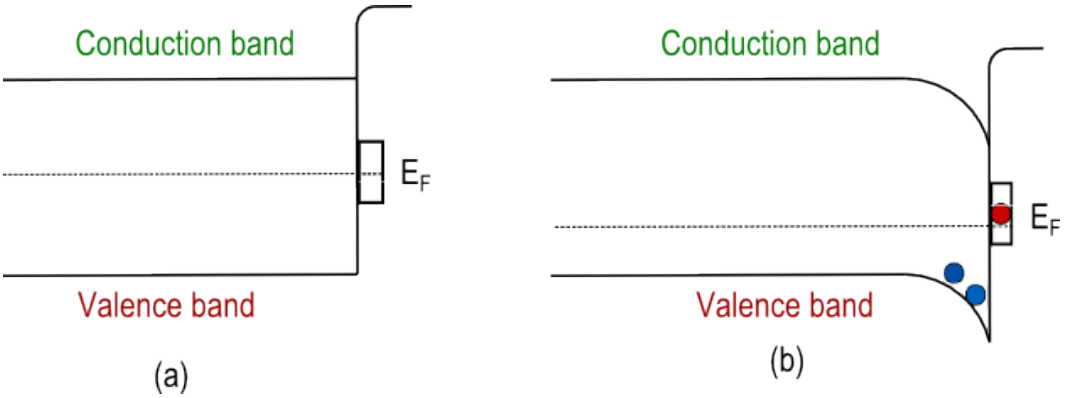

Figure 2.5: a) Intrinsic GaAs, Fermi level in the middle of the band gap. b) GaAs with P doing. Fermi level moves towards the valence band creating band bending region at the surface. Blue represents electrons and Red represents holes.

The properties of the doping material can change the surface potential dramatically. If the doping is P type, the acceptors from the dopant will combine with the electrons on the surface states and the surface will have a positive charge. To restore charge neutrality, the region immediate to the surface will become negatively charge. The Fermi level on the surface should lie in the

middle of the band gap at the surface since the surface is charge neutral. P type doping shifts the Fermi level towards the valence band in the bulk of the material. Therefore to keep the Fermi level at the middle of band gap at the surface, the valence band will experience a bend towards the surface. This region is called the depletion region and the thickness of depletion region is given by

$$l = \sqrt{\frac{2\epsilon V_{bb}}{qN_a}} \tag{2.2}$$

Where V_{bb} is the band bending potential, ϵ is the dielectric constant and N_a is the impurity concentration. A wide depletion region is not desirable since it reduces the probability of electron escape due to increasing electron-phonon scattering. From equation 2.2, depletion region can be made shorter by using high concentration of impurities. On the other hand, too high doping concentration can cause spin relaxation by reducing the diffusion length. A balanced doping concentration has to be used to maximize both the escape probability and spin polarization of the emitted electrons. A doping concentration of 10^{18} cm^{-3} is used commonly to achieve a depletion region of 100 A^o [37].

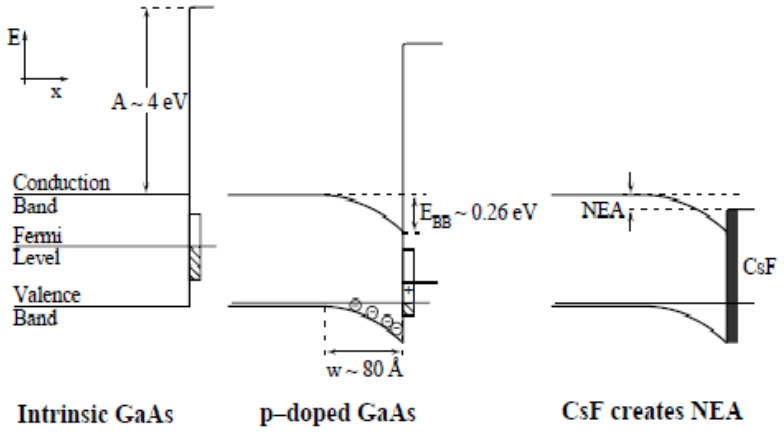

Figure 2.6: Cs-Oxidant layer creating NEA at GaAs surface

Scheer first discovered that depositing Cs on cleaved GaAs surface increases QE substantially [11]. Later it was discovered that addition of an oxidant (e.g. oxygen, NF_3 etc.) can increase the QE even more [3]. Figure 2.2.2 shows NEA creation on P-doped GaAs. The deposition of Cs and Oxygen could be

simultaneous or 'yo-yo' and described in detail in chapter 3. The final QE does not seem to depend on the method of Cs-O deposition [37].

2.2.3 Polarized electrons

In 1975, Pierce[38] first proposed that NEA GaAs can be used a source for polarized electrons. The first measurements of electron beam polarization was published in 1976 by the same group showed that polarization shows a peak of 40% from transition at Γ point corresponding to energies close to band gap[3] .

Figure 2.7 shows the transitions in GaAs at the Γ point. The splitting of the P band at Γ point due to spin-orbit coupling into $P_{3/2}$ and $P_{1/2}$ level plays a key role in obtaining polarized electrons from GaAs. The direct band gap is also very important since this property allows transitions between states that has well defined angular momentum at Γ. When GaAs is irradiated with right(left) circularly polarized light with energy between E_g and $E_g+\Delta$, the only possibly transitions are for states such that $\Delta m_j = m_f$ - m_i = 1(-1).

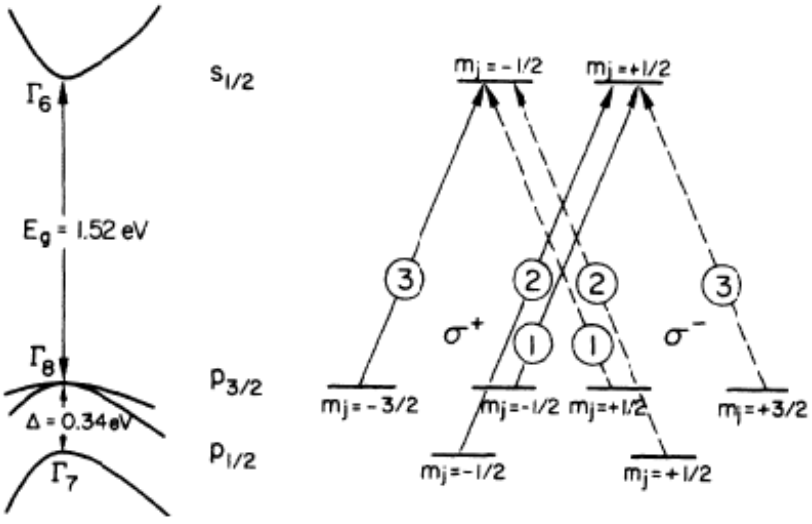

Figure 2.7: The band structure of GaAs at Γ point on the left. The allowed electromagnetic transitions with corresponding probability values are shown on the right [3].

From figure 2.7, it is clear that the maximum achievable polarization from bulk GaAs is (3-1)/(3+1) × 100% = 50%. As the energy of the incident photon gets higher, the polarization decreases due to transition from the split off band

to the conduction band with a transition probability of 2. In practical cases, the achievable polarization from bulk GaAs is limited to 40% due to lattice imperfection and inelastic scattering of electrons [39]. For polarization higher than 40%, strained GaAs is used where the degeneracy of the valence band is broken. CEBAF at JLab uses strained superlattice GaAs for 1% QE at 800 nm and 80% polarization.

2.3 Operating GaAs in a DC gun

All the existing polarized electron beam facilities in the world use a DC gun as the source. In DC guns, the electrons get accelerated by traveling from lower potential to higher potential in a constant electric field. The acceleration voltage can range from 60 KV to 350 KV depending on the required beam parameters and gun geometry. Using GaAs in a normal conduction RF gun has proved to be difficult due to poor vacuum and multipacting issues [40]. There has not been a thorough study of GaAs operation in a SRF (Superconducting RF) gun [41]. For this experiment, we used a DC gun and hence we will focus our discussion on the various aspects of GaAs cathode performance in DC guns.

2.3.1 Vacuum contamination

The importance of impeccable vacuum for GaAs cannot be overemphasized. The Cs-O layer that creates NEA is extremely sensitive to vacuum and any active contaminants can degrade the NEA layer over time. Rodway [42] proposed that the loss of QE for activated GaAs is due to either loss of Cs or gain of O_2. Dedicated experiments where active contaminant gases such as O_2, CO_2 and CO were introduced in a chamber containing an activated GaAs cathode [43] and the decay of QE was measured. The decay was found to be exponential and the time constant for this exponential decay is defined as the 'lifetime' of a photocathode. This lifetime is inversely proportional to the partial pressure of different gas species such that

$$\tau = \frac{\kappa_i}{P_i} \tag{2.3}$$

Where i denotes different gas species, κ_i is the proportionality constant that varies from species to species (e.g. κ_{O_2} is 1.5×10^{-6} s.mbar) and P_i denotes the partial pressure for the specific gas species. So in order to have a stable vacuum condition for long enough lifetime of activated GaAs, the partial pressure for

the above mentioned gases has to be lower than 10^{-12} Torr. It was also noticed that reactivation with Cs can restore the QE of the cathode, however the lifetime seems to be shorter with each Cs activation cycle [44].

If a gun is to be used as a polarized source, the static and dynamic vacuum needs to be good. This is a clear advantage that DC guns have compared to normal conducting Copper RF guns. A DC gun is generally made out of Stainless Steel which has a much lower outgassing rate compared to Copper. Even with the right choice of material, rigorous baking procedure and careful design of vacuum components has to be implemented in order to achieve low 10^{-11} Torr level vacuum.

2.3.2 Field emission

Field emission in the DC gun can generate unwanted gas load that contaminate the cathode and shorten the lifetime. Before a DC gun is used for beam operation, generally it is high voltage conditioned for a long time to reduce field emission currents. The high voltage conditioning process generally constitutes of bring up the voltage in the system gradually and measure the current in the DC gap. For a field emitter, the current should exponentially increase with increasing voltage accompanied by radiation that can be detected using radiation detectors. JLab measured pico-ampere level current between the cathode anode gap with a biased anode which resulted in excellent lifetime [15]. As a general rule, field emission current should be lower than 100 nA for 100 hours of lifetime in the gun. High voltage conditioning process is discussed in detail in chapter 3.

2.3.3 Ion back bombardment

Photocathode damage during operation by ion back bombardment was first reported by Mainz [45]. In this process, the residual gas between the cathode anode gap gets ionized by the electron beam and essentially traces back the electrons path towards the cathode. Ions can hit the cathode with sufficient kinetic energy to sputter away the Cs-O layer. This will result in cathode losing NEA on the surface and less current for a fixed laser power. In a circular configuration, the ions would damage the electrostatic center of the cathode. A schematic diagram showing ion back bombardment is shown in figure2.8. For a fixed acceleration potential, the lifetime due to ion back bombardment should be inversely proportional to the current, the residual gas pressure in the system and should be directly proportional to the beam area or laser spot area [14]. It can be written as

$$\tau_{ibb} \propto \frac{A}{P_{res} I} \tag{2.4}$$

Where τ_{ibb} is the ion back bombardment dominated lifetime, P_{res} is the residual gas pressure and I is the current. Therefore the higher the average current, for a fixed spot size and fixed vacuum, the lower will τ_{ibb} be. The charge lifetime, Q_τ, can be found as

$$Q_\tau = \tau_{ibb} I \tag{2.5}$$

Equation 2.5 shows that charge lifetime is directly proportional to the laser spot size. That would imply that with increasing laser spot size, the charge lifetime should increase. Even though this phenomena is observed with increasing laser spot sizes [15], the relation between laser spot size and charge lifetime is not linear.

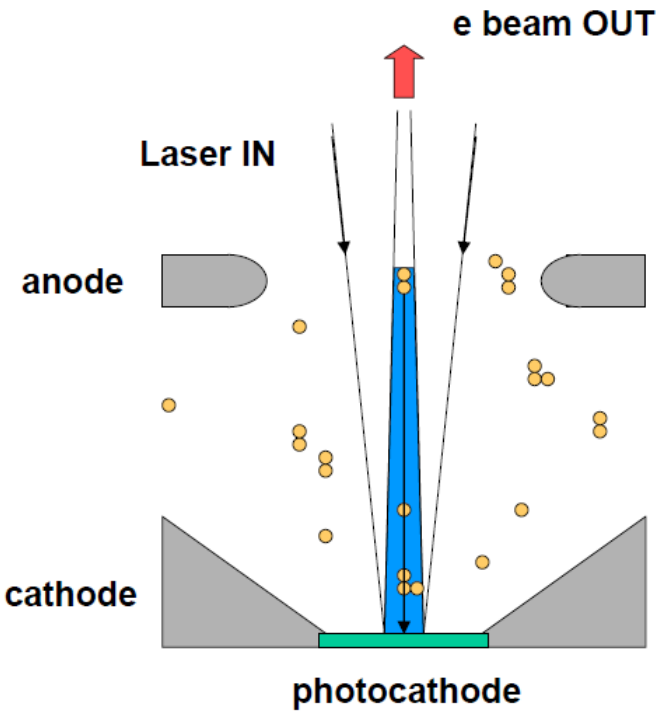

Figure 2.8: Ion back bombardment in DC guns. Electrons ionize residual gas molecules in the gap that gets accelerated towards the cathode [4].

At pressures below 10^{-11} Torr, the dominant gas species in a vacuum sys-

tem is H_2. The ionization cross section of H_2 is much lower for electron energies over 100 KeV [46]. For DC guns with voltages in the 100 KV range, it means that most of the ions can be generated in the DC gap and very close to the cathode. This problem can be partially solved by designing DC guns that are capable to operate at a higher voltage.

Another idea to manage ion back bombardment damage on the cathode is to extract beam off-center of the cathode. If the damage is on the cathode center but beam is extracted from a spot that is away from the center, the cathode would survive longer and would have higher charge lifetime. CEBAF gun employs this idea and shown to have better charge lifetime compared to operating from the center of the cathode [15].

The inevitability of ion back bombardment makes mA operations particularly challenging. The charge lifetime for 4 mA test at JLab was 80 coulombs or 5.5 hours of continuous operation. For even higher currents, e.g. eRHIC requirement of 50 mA, lifetime would be even shorter. To complicate things further, laser power required to generate 50 mA average current would be 80 W for 1% QE and would heat up the cathode. GaAs starts to lose the NEA layer at temperatures over 60 ^{0}C. The gun will have to equipped with cooling system to keep the GaAs at room temperature.

A solution towards higher currents with acceptable charge lifetime could be combining multiple beams from multiple cathodes. If the charge lifetimes of the cathodes are independent of each other and ion back bombardment is the dominating factor, adding cathodes to the source should add the charge lifetimes. Grames et al. [15] showed that charge lifetime per unit area for a gun for a specific set of operating conditions would be a constant. That means for a fixed laser spot size and operating condition – high voltage, field emission current, static and dynamic vacuum– the charge lifetime of a gun is a constant value. Now consider two electron guns that are independent and vacuum separated. If they were to be combined in such a way that the combination procedure does not interfere with the individual gun operation, the charge lifetime of the source should be the sum of the individual charge lifetimes. For the combined charge lifetime, one can then chose what average current to operate the source. Since charge lifetime is a constant, choice of operational average current then should determine the operational lifetime for the source.

To understand this concept, we can use the results from Jlab's 4 mA av-

erage current operation [22]. In this experiment, 4 mA operation from one cathode yielded 80 C with 5.5 hours of operational lifetime. So for the particular laser spot size, we assume, that this gun is capable of producing 80 C of charge. If two guns that are exactly the same as the gun used in this experiment were to be combined, the charge lifetime of the source should be 160 C. Now that the total charge lifetime is known for a fixed laser spot, the average current can be chosen and the operational lifetime can be determined. For 8 mA average current after beam combination, each gun would have to operate for 5.5 hours. For 4 mA average current, each gun would operate at 2 mA for 11 hours keeping the charge lifetime constant.

In practice, operation of multiple single cathode gun could be problematic. They each would require their own cathode preparation chamber, high voltage power supply and beam optics. This issue can be solved if multiple cathodes can be operated from the same vacuum chamber. If the operation of one cathode is independent of the operation of other cathodes, then only one gun can be used to operate multiple photocathodes and then combine the beams. The beams can be combined using a rotating magnetic field with the same frequency as the laser repetition rate. The rest of the dissertation describes the design of such a gun, where 20 cathodes can be operated in the vacuum chamber. Results from two beam combining test are also presented in Chapter 4. The results show that the ion back bombardment dominated charge lifetimes can be added using two cathodes in the same vacuum chamber.

Chapter 3

Experimental Setup

Combining multiple beams into one common axis can extend the charge lifetime of the source and can possibly be used a high current source for practical collider applications such as eRHIC. In order to test the beam combining scheme, a multiple cathode gun is required. Keeping this in mind, the collider accelerator department designed a multiple cathode gun that combines the beams using a rotating magnetic field [47]. The gun is unique in its capability to house 20 cathodes that run sequentially, and combine the beams downstream with a rotating magnetic field. [48]. The cathodes are located in the same chamber, they are not vacuum isolated. This configuration allows the experiment of cathode 'cross-talk' which would explain whether or not the operation of one cathode is independent of the other.

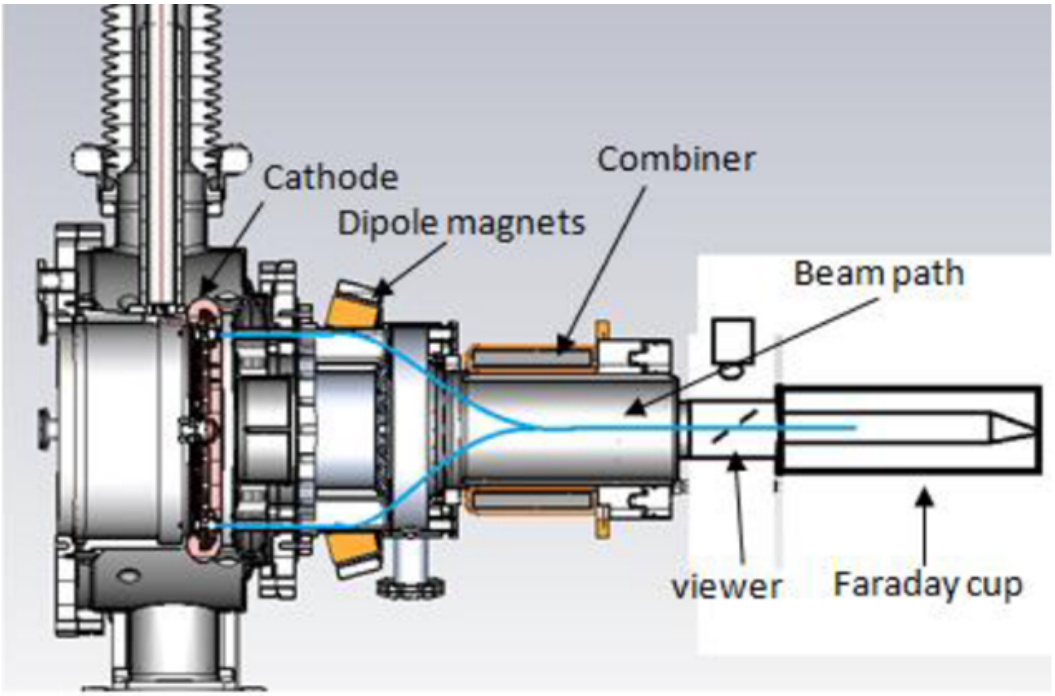

Figure 3.1: Cross sectional view of the gun showing the trajectory of two diagonally opposite beam being combined at the combiner.

The gun system can be divided into two major subsystems: cathode preparation-transfer section and the gun section. The cathode preparation-transfer section includes the load-lock section, the preparation chamber and the transfer line. The gun section includes cathode loading section, high voltage section, beam transport section including beam optics and Faraday cup.

3.1 Cathode preparation and transfer section

GaAs cathodes have to be activated before they are installed in the gun for beam extraction. The activation procedure involves evaporation of Cs in the chamber and introducing O_2 to achieve negative electron affinity (NEA). If the cathodes were to be activated in the gun chamber, the Cs might stick to the wall of the high voltage gap and could cause field emission. Any residual O_2 would only poison the NEA layer. A preparation chamber separated from the gun chamber by a valve solves these problems.

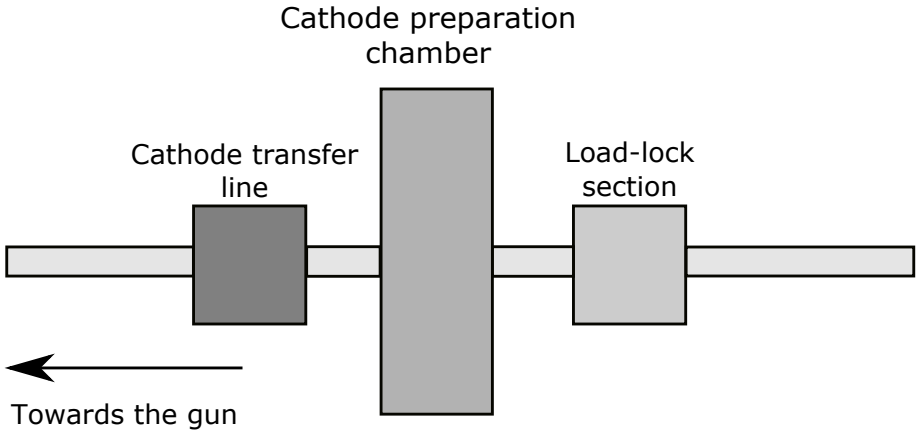

Figure 3.2: Schematic diagram showing components of cathode preparation-transfer section.

A load-lock section for fresh samples is also an essential. Since the preparation chamber requires 10^{-12} Torr vacuum, exposing it to air to load new samples could contaminate the chamber. Having the preparation chamber under vacuum at all times is a good practice for reliable cathode production. A load-lock chamber, dedicated to only cathode loading, ensures that the preparation chamber is never opened.

3.1.1 Load-lock and transfer manipulator

The load-lock chamber is a standard 2.75 inch diameter 6 way stainless steel cross. A schematic diagram of the load-lock system is shown in figure3.3. Two

custom made 'placeholder' structures are installed on opposite flanges. One port of the cross is connected to the preparation chamber via an all metal valve. The opposite flange of the valve has a 5 meter long, commercially available, magnetically coupled transfer manipulator. The top port of the cross has a window to observe cathode transfer between the manipulator and placeholders. A 20 l/s ion pump is located at the bottom flange. The ion pump has a side port to attach a roughing-turbo pumping station when necessary.

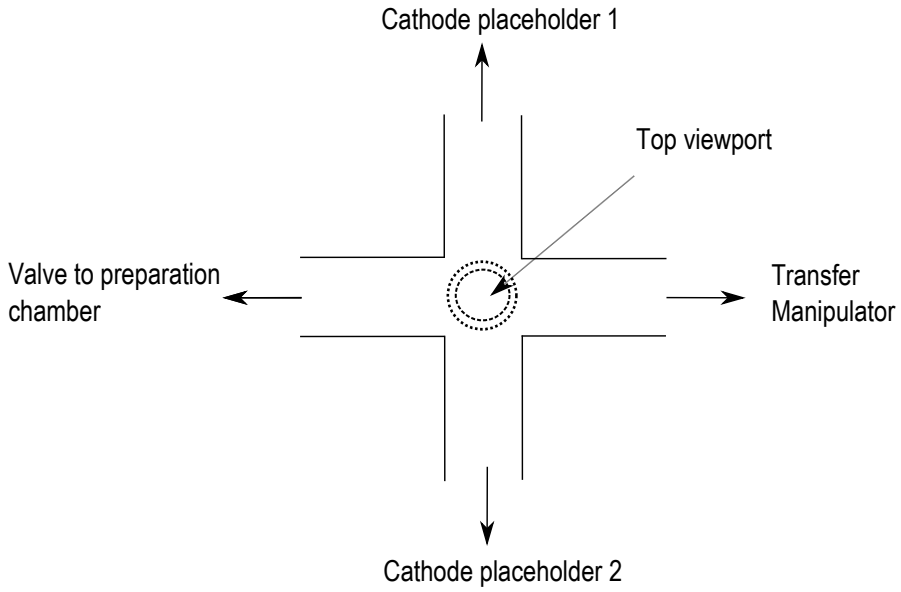

Figure 3.3: Schematic top view of the load-lock chamber. The bottom flange connected to the ion pump is not shown.

When a fresh set of GaAs samples are loaded in the load-lock, it is valved off from the preparation chamber and baked separately afterwards to establish good vacuum. Even though this section does not have a vacuum gauge, the ion pump current can be monitored to know when the valve can be reopened.

3.1.2 Cathode preparation chamber

Structure and vacuum components

The cathode preparation chamber is a compact structure capable of achieving extreme high vacuum (XHV) level, pressure below 10^{-11} Torr, consistently. The XHV structure is three standard 2.75 inch Stainless Steel crosses stacked one on top of another. Two of these crosses are 6 way crosses and the remaining one is a 4-way cross. The 4-way cross is at the bottom and the other two crosses on top of the bottom one. Figure 3.4 shows a schematic diagram of the preparation chamber with its various components. Different vacuum components are listed in Table 3.1 and 3.2.

Pump type	**Pumping speed**
Ion Pump x 2	120 l/s
Non Evaporable Getter x 2	200 l/s

Table 3.1: Vacuum pumps on the cathode preparation chamber

Gauge type	**Measurement range**
Convectron Gauge	Atm. to 1×10^{-4} Torr
GP hot filament ion gauge	1×10^{-4} - 1×10^{-9} Torr
ULVAC Axtran gauge	1×10^{-8} - 5×10^{-12} Torr

Table 3.2: Vacuum gauges on the cathode preparation chamber

The Cs source used in the chamber is an evaporation Cs source from SAES Getters Inc. O_2 is introduced into the chamber via a leak valve. A vertical manipulator is used for vertical movement of the cathode holder.

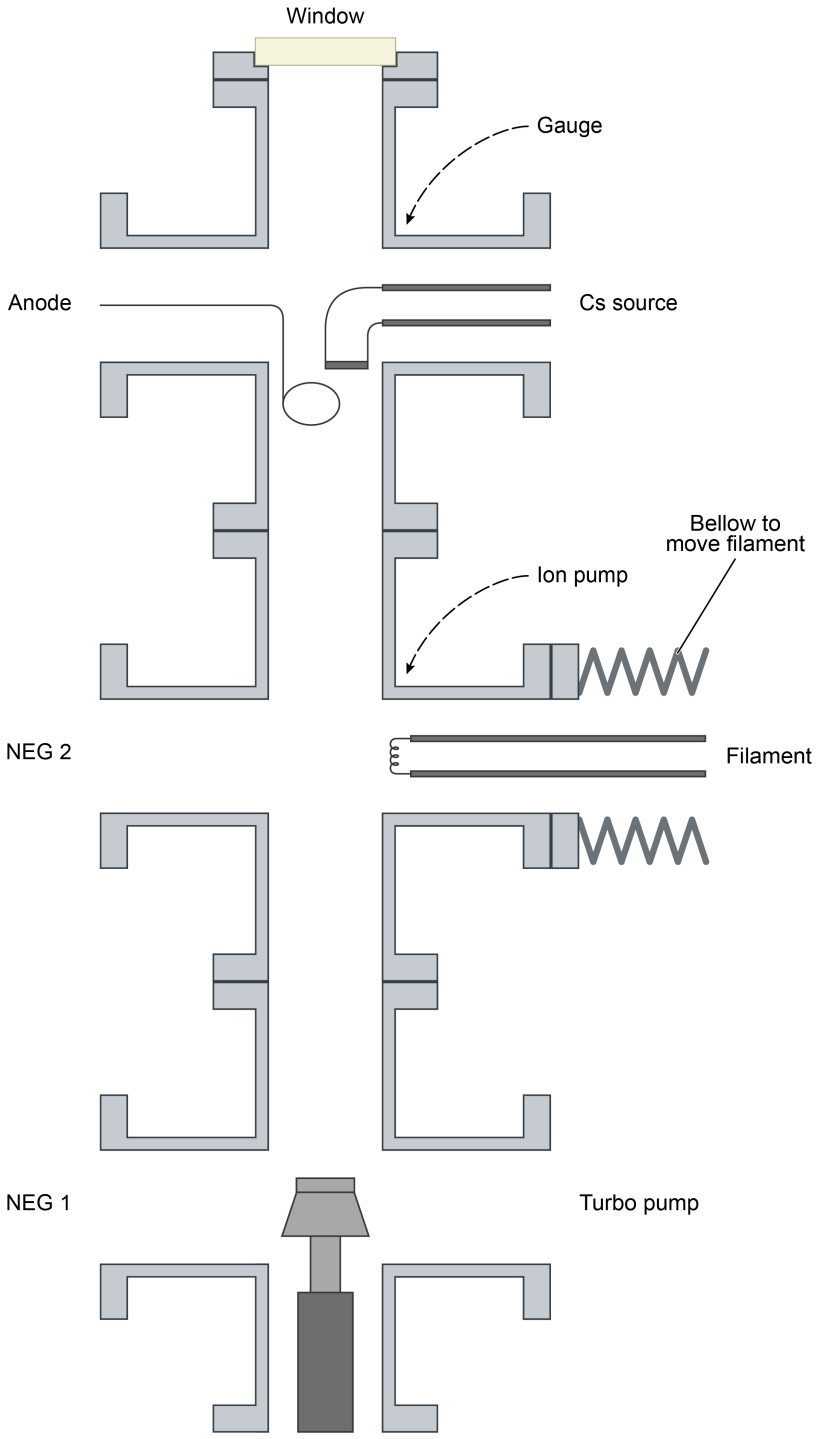

Figure 3.4: Schematic diagram of the preparation chamber showing various components. The cathode holder is moved up and down by a vertical manipulator.

Bakeout procedure and vacuum performance

The bakeout procedure for the preparation chamber has turnaround time of 7 days. Step by step standard bakeout procedure is as following:

1. Roughing pump and turbo pump to bring vacuum in the chamber to 1×10^{-6} Torr.

2. Use standard heater tapes around the chamber, aluminum foil for uniform thermal coverage. Multiple thermocouples are attached to the chamber to measure temperature.

3. Bring the temperature of the chamber up from room temperature to 50^0C to 120^0 C.

4. Activate the NEG pumps into the turbo pumps when the chamber is at 120^0C. Degas the ion pumps, the Cs source, the cathode holder and the gauges.

5. After degassing all the components, increase the temperature to 200^0C. The pressure will rise for a day and then drop slowly.

6. When the pressure of the system is not dropping more than 15% over 24 hours, the cool down begins.

7. Cool down is slow to avoid leaks. Chamber is brought down from 200^0C to 80^0C over two days.

8. At 80^0C, activate the NEG pumps and degas the Cs source and the cathode holder into the turbo. Then Valve off the turbo and let the chamber cool to room temperature.

The leak valve for the oxygen is kept open during the chamber bakeout. After the chamber has achieved its final pressure, the leak valve is closed and attached to the oxygen tank using a stainless steel line. The leak valve and oxygen line assembly is then baked into a turbo at 120^0C - 150^0C. This procedure is crucial to ensure that the ultra high purity oxygen from the tank does not get contaminated by water or any active gases as the leak valve is filled.

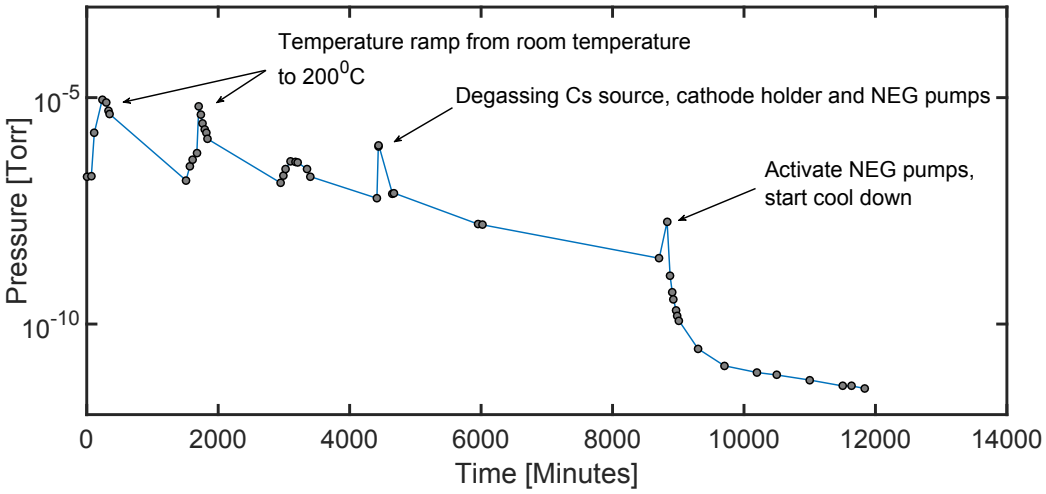

Figure 3.5: Typical bakeout performance of the cathode activation chamber.

Heat cleaning

Good QE GaAs cathode requires an atomically clean surface. During the bake-out, contaminants might stick to the surface of the sample. That is why sample surfaces are cleaned before every activation. The most widely used method of cleaning the surface is by heating up the sample to a desired temperature. The temperature of heat cleaning should be regulated since underheating will result in an unclean surface and overheating might damage the crystal permanently.

To determine the optimum heat cleaning temperature, we measured the QE of a bulk GaAs for different heat cleaning temperatures. The results are shown in figure 3.6. The maximum QE at 650 nm was found to be the 590^{o}C heat cleaned sample. For temperatures below 570^{o}C and above 610^{o}C, the QE's were low. For the cathodes during beam test, we heat cleaned the cathodes at 580$\pm$5 ^{o}C. For heat cleaning the GaAs sample, the cathode holder is moved up to the heating position (figure 3.8). A Tungsten filament, extracted from a 250 watt light bulb, is used to heat the sample in the preparation chamber. The filament can be moved back and forth inside the chamber by a mechanical bellow. The temperature of the surface of the GaAs samples were calibrated against the input power of the filament for a fixed filament position and fixed vertical manipulator position.

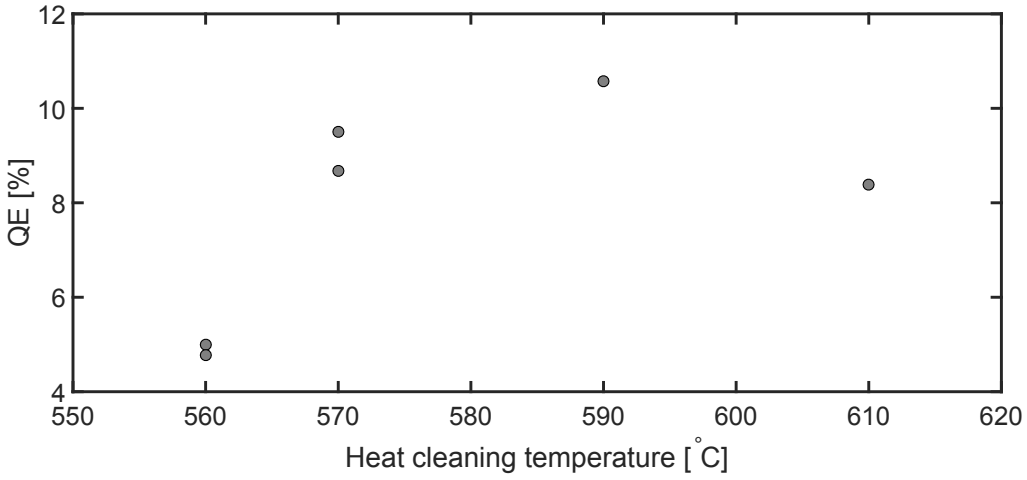

Figure 3.6: QE, for 650 nm, for different heat cleaning temperature of the sample.

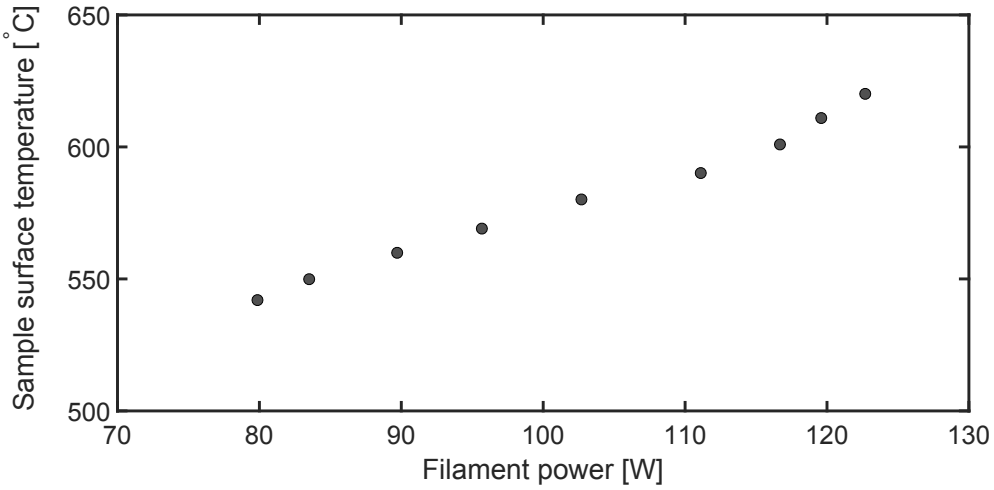

Figure 3.7: Surface temperature calibrated against the filament output power.

After the sample has been heat cleaned for 45 minutes, it is left to cool down back to room temperature. Immediately after the sample heater is turned off, the Cs source is degassed for a 2-3 minutes. This is because during the sample cleaning procedure, the Cs source is cold and can potentially have gas molecules from the sample stick to it's surface. If the Cs is not degassed properly, then the first burst of gas from the Cs during activation will contaminate the surface of the sample and essentially negate the cleaning procedure.

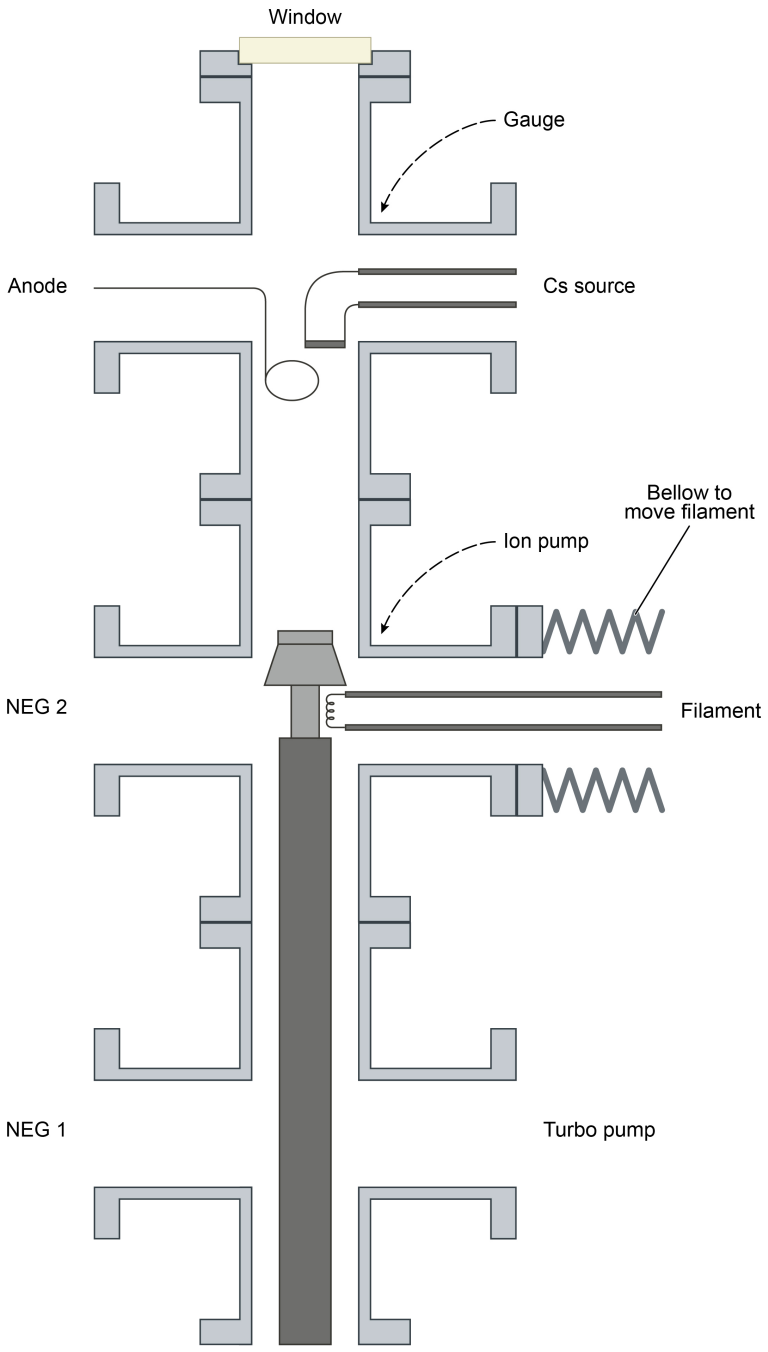

Figure 3.8: The cathode holder in the heating position inside the preparation chamber. The heating filament is moved underneath the cathode holder using the mechanical bellows.

Cathode activation

It takes 2.5 hours for the sample to cool down to room temperature. We used co-deposition method, simultaneous deposition of Cs and Oxygen, to activate the sample. During the Cs-O_2 co-deposition, the photocurrent is measured using a pick-up anode. Using the wavelength of the laser, laser power and photocurrent, QE during activation can be calculated as

$$QE = \frac{1.24}{\lambda(\mu m)} \times \frac{I}{P} \tag{3.1}$$

Where λ is wavelength in μm, I is the measured photocurrent and P is power of the laser.

The steps of activation are :

1. The cathode holder is moved up from the heating position to get closer to the anode and Cs source.
2. Position the laser on the cathode surface. The laser used for activation is 650 nm laser pointer with 1.2 mW of full power.
3. Bias the anode to 75 Volts to pick up photo-electrons. The electronics is set up such that the current picked up by the anode is measured by measuring the voltage drop across a 10 MΩ resistor.
4. Turn on the Cs source. A 6 amp current flows through the Cs source. The current value is obtained from the calibration curve provided by the vendor and previous experience on this particular chamber.
5. The Cs source would take about 30 seconds to heat up. The Cs source heating can produce current on the anode. To confirm photoemission, turn the laser on and off to see if there is a change in current signal.
6. Approximately 5 minutes later, signal from photoemission is observed. As the signal is increasing, use a 10x neutral density filter to lower the laser power. This is done to avoid the space charge limit in the chamber.
7. After the Cs peak, the signal will start to fall. Wait for the signal to fall 25% of its Cs peak value. At that point, the oxygen is introduced in the chamber. The oxygen introduction is slow and regulated.
8. Increase the oxygen leak rate until a steady rate of signal increase is achieved and monitor the photocurrent.

9. After some time, the signal will be steady. Try adjusting the oxygen leak rate to see if there is change in the signal. If the signal is decreasing for both increasing and decreasing Oxygen, turn the oxygen off.

10. Turn the Cs source off, measure the final current signal.

A sample activation curve using a 650 nm laser is show in figure 3.9.

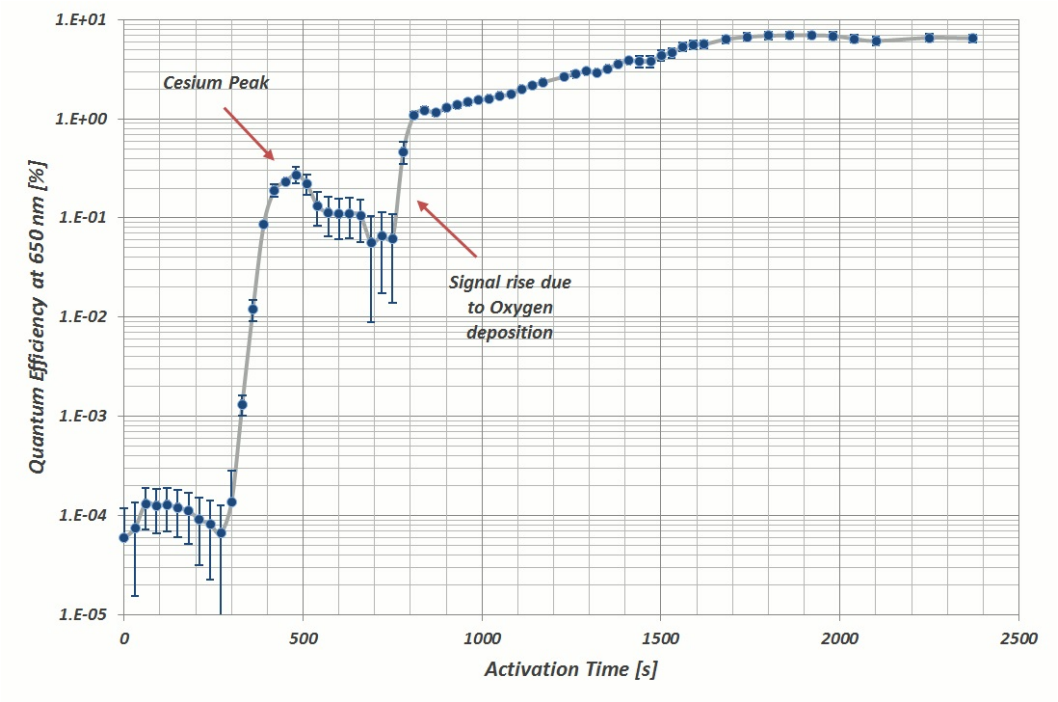

Figure 3.9: A typical activation curve for bulk GaAs in the cathode preparation chamber.

3.1.3 Transfer line

The transfer line section that attaches the gun to the preparation chamber is a Titanium tube with a welded 4 way cross in the middle. The vacuum level in this section is needed to be very low to preserve the quantum efficiency of the photocathode during transport. The 4 way cross includes a 20 l/s Ion pump, a Capacitorr D 400 80 l/s NEG pump and a hot filament gauge to monitor the pressure. The Transfer line is vacuum isolated on both ends by VAT all metal valves. During the initial bakeout, the transfer line is baked along with the preparation chamber. After a week of baking, the measured pressure was 4×10^{-11} Torr.

3.2 The Gun

The unique capability of the funneling gun is that it can operate 20 cathodes at a time. The main components of the gun assembly are: Cathode loading chamber, high voltage section, beam optics section and beam diagnostics section.

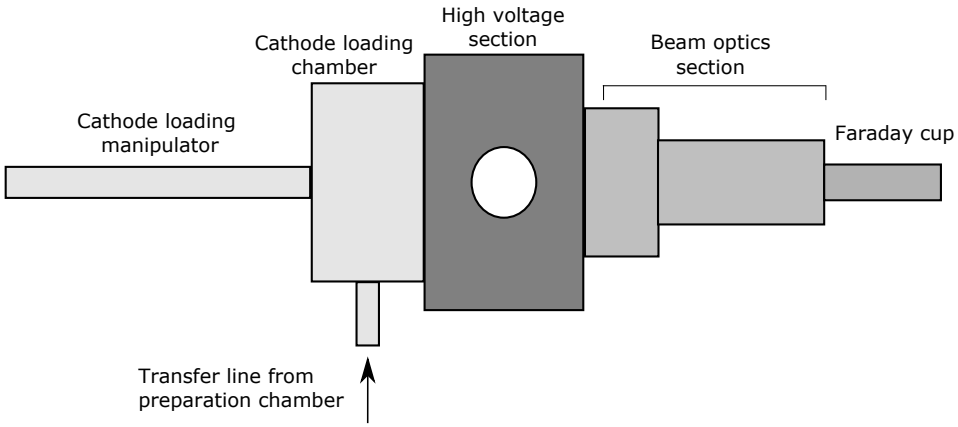

Figure 3.10: Schematic view of the gun from top. The circle on the high voltage section indicates the ceramic feedthrough flange.

3.2.1 Cathode loading section

An activated cathode from the preparation chamber is transferred to the cathode loading section to be loaded on a circular magazine that holds twenty cathodes. The circular magazine is controlled using a magnetic manipulator. Once the cathodes are loaded in the magazine, it is moved forward towards the high voltage shroud and locked in place using a lock at the back of the magazine.The vessel has two 16" diameter flanges. It is attached to the main gun chamber on one side and has the cathode magazine manipulator on the other end.The vessel and the magazine are both vacuum fired 316L stainless steel. Pumping in this section include an all metal valve insulated port to a turbo pump, 100 l/s ion pump and 2000 l/s Titanium sublimation pump.

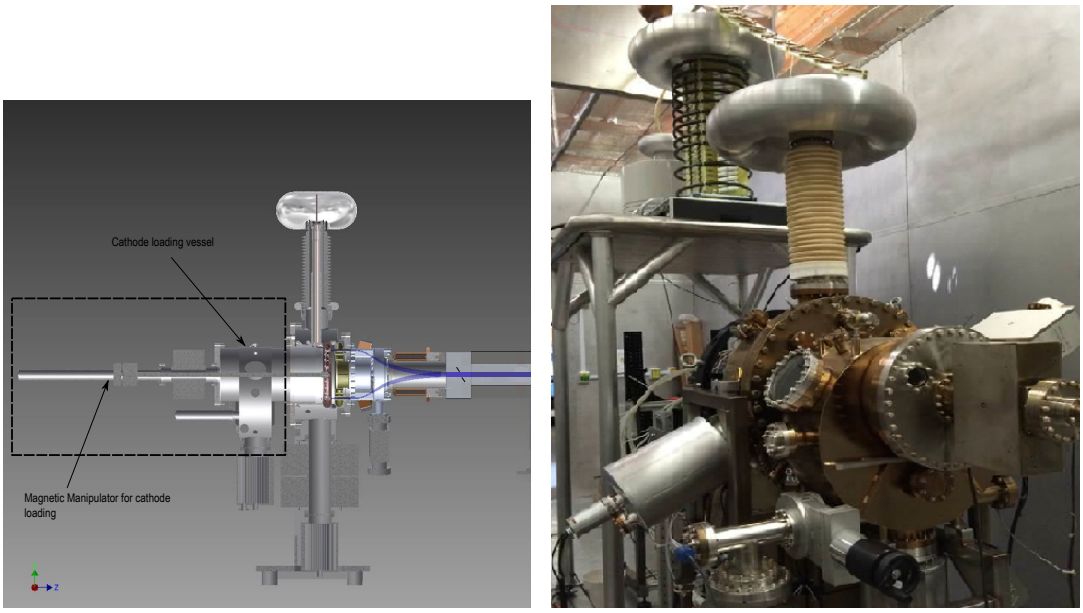

Figure 3.11: Left: The cathode loading section on the gun structure. Right: Photograph showing the cathode loading vessel.

3.2.2 High voltage section

The high voltage section consists of main gun vessel, cathode shroud and anode assembly. The gun vessel is a vacuum fired 316L Stainless Steel chamber with two 22" flanges at the front and back. The back of the vessel is connected to the loading chamber. The front end of the gun vessel is attached to the fixed dipole holder structure.

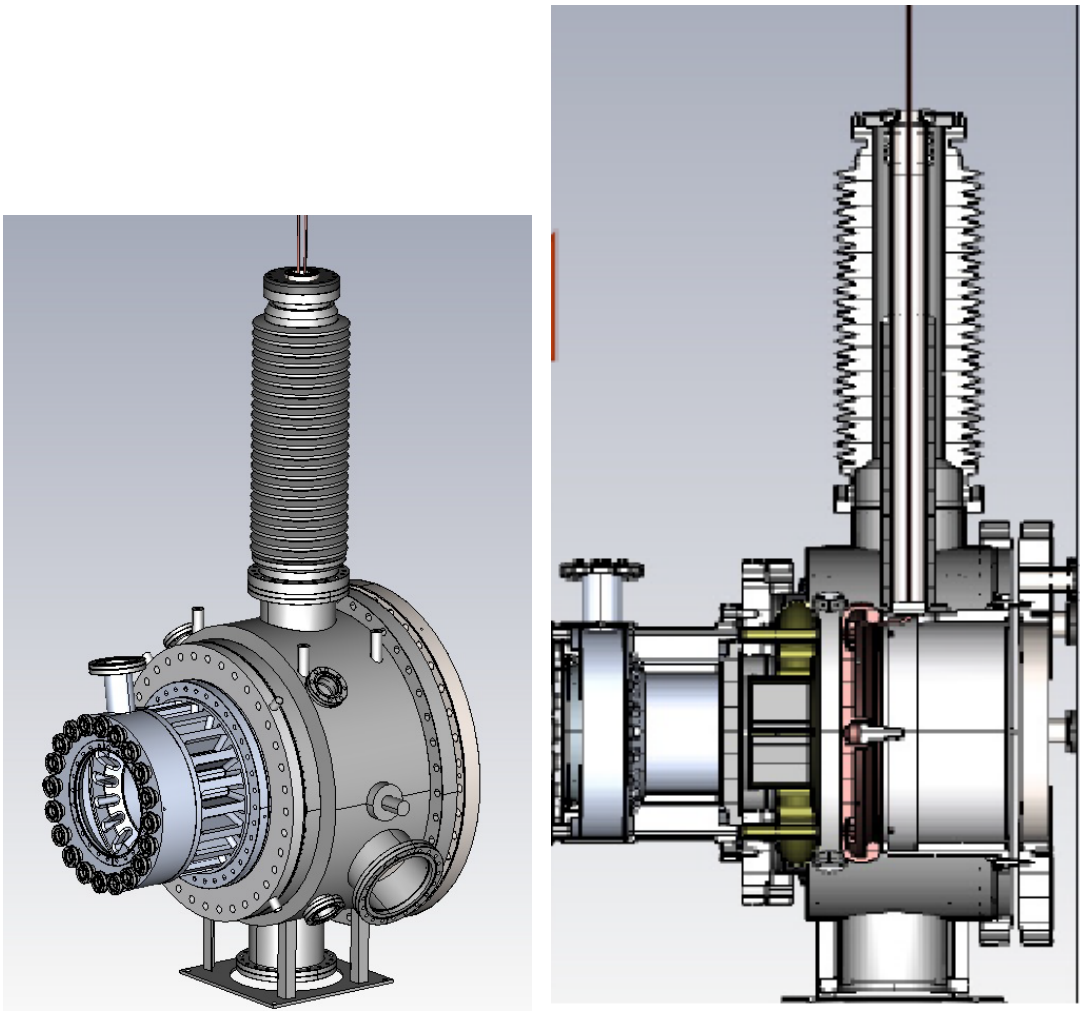

Figure 3.12: Left:The high voltage vessel with the ceramic on top. Right: Cross sectional view of the cathode shroud.

The cathode shroud is polished 316L Stainless Steel. The cathode shroud is mirror finished to prevent field emission between the DC gap. The anode structure is made from Titanium. Titanium has an outgassing rate an order of magnitude less compared to Stainless Steel. This would minimize the outgassing from the anode from any stray electrons.

The cathode shroud has a copper block with cooling lines brazed to it at the back. The cooling lines can be used to actively cool the cathodes during mA current operations. It is connected to the top flange by a stainless steel feed-through, which is also the connection to the high voltage power supply.

To ensure good vacuum in the cathode-anode gap, a custom made TSP from Atlas industries, WA, was installed in the middle of the anode structure. This particular TSP has an artichoke structure to maximize the Ti sublimation surface area. The artichoke structure also prevents Ti to get into the DC gap.

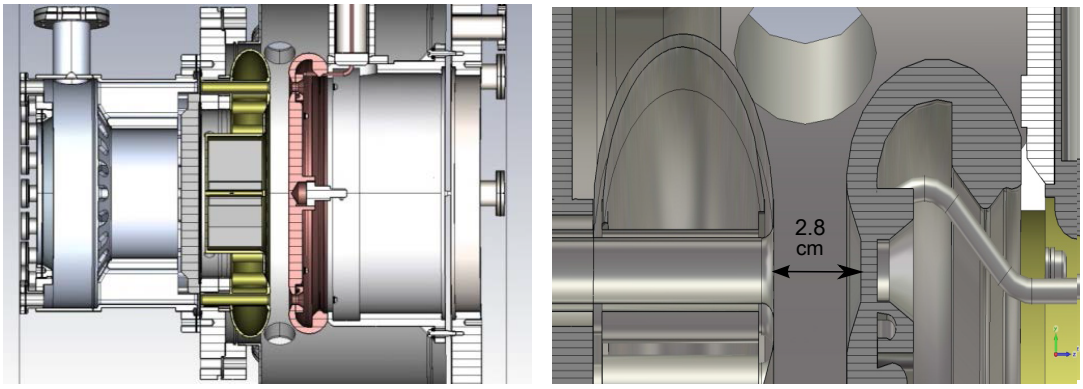

Figure 3.13: Left:The high voltage vessel with the ceramic on top. Right: The polished cathode shroud that is located inside the high voltage vessel.

3.2.3 Beam optics section

The beam optics design and beam dynamics simulation for the gun was done by X. Change et al.[47] and E. Wang et al.[49]. This section overviews the main components of the beam optics section.

After the electron beams are extracted and then accelerated in the DC gap, they encounter the beam optics section where they get bent twice. In order to preserve the initial polarization of the cathodes, the bends would either have to a pair of electric bend or a pair of magnetic bends. A pair of magnetic bends were chosen because of the ease of implementation for 250 KeV electron beams. The first bend after the anode section is a fixed dipole bend and second bend is a rotating dipole bend.

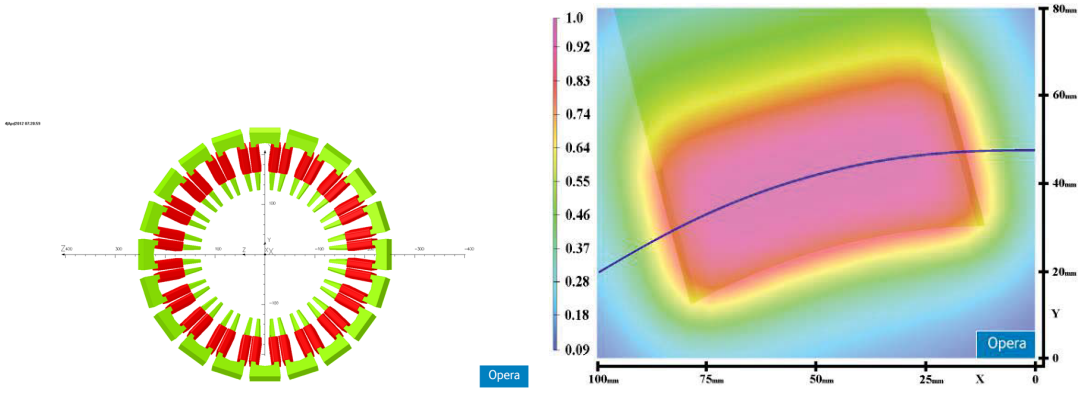

Figure 3.14: dipole simulations

The fixed bending magnets are mounted on an Aluminum structure with slots for twenty individual magnets. The magnets are outside the vacuum chamber and can be tuned for each individual beam. The optimized bending angle for these magnets are 30 degrees.

After the fixed dipole bend, individual bunches approach the combiner magnet where a rotating magnetic field bends the bunches to its axis. The individual cathodes are radially distributed on a circular cathode shroud. Two neighboring cathodes are separated by 18 degrees. If all 20 cathodes were to be operated by extracting beams sequentially, the combiner must have the right dipole field for each cathode to combine them to its axis. That means the combiner field must rotate from cathode to cathode as the individual bunches are arriving at the combiner. A rotating dipole magnetic field can be generated by using a continuous cosθ current distribution on a cylindrical surface. For all practical purposes, a discrete quasi-cosθ distribution can be used to obtain a uniform dipole field in the middle of the cylinder. Therefore, the current on the dipole coils for a combiner field can be written as [50],

$$I_D = I_{0D} cos(\omega t + \Phi_D) \tag{3.2}$$

Where I_{0D} is current on the dipole coil, $\omega = 2\pi f$ is the angular frequency of rotating and Φ_D is the orientation of the dipole coil with respect to the combiner axis central horizontal plane. A flux plot of the dipole field, simulated in Opera, is shown in figure 3.15. 12 dipole coils and a ferrite core were used to simulate the field.

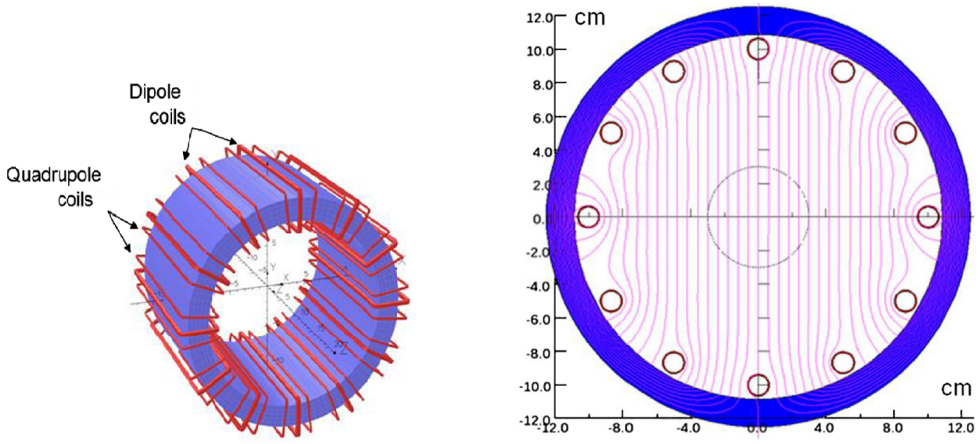

Figure 3.15: Combiner dipole field flux plot showing uniform dipole field at the center of the combiner. 12 dipole coils and a ferrite core was used.

In order to compensate for the unequal emittance growth on the two transverse direction, a set of quadrupole coils were wound on the combiner ferrite core. The quadrupole currents can be written as

$$I_Q = I_{0Q} cos2(\omega t + \Phi_Q) \tag{3.3}$$

Where I_Q is the amplitude of the quadrupole current, ω =2πf is the rotation frequency and Φ_Q is the orientation of the quadrupole coil with respect to the horizontal plane of the combiner axis. Figure 3.15 also shows the dipole and quadrupole windings on the combiner ferrite. The time dependence of I_D and I_Q, from equation 3.2 and 3.3 respectively, makes it possible to rotate the fields with advancing time. The ultra high vacuum requirement for the polarized source requires that the combiner be isolated from the vacuum chamber. A uniform field distribution in the middle of the combiner component is essential for beam combining. To fulfill both the criterion, a ceramic tube acts as the vacuum tube for beam propagation and the combiner ferrite is slid over it. Ideally the ceramic tube should have been coated with a very thin layer of conductive material to prevent charge build up, without screening the magnetic field. For this set of experiment, a 100 micron thick Titanium foil was used instead of the conductive coating.

The power loss in the combiner magnet was calculated to be 600 W for 200 KeV electron beams. Low loss and fast response ferrite MN8CX was chosen to be the core material. The ferrite was also segmented to increase the surface area to help cool the magnet. Copper cooling lines are part of the ferrite

structure so that the ferrite can be water cooled.

3.2.4 YAG and Faraday cup

A YAG crystal is used for viewing the beam and is located downstream of the combiner magnet. The crystal is held by three aluminum rods from the Faraday cup. There is a hole in the middle of the crystal such that beam can be tuned to go through the hole directly to the Faraday cup. The Faraday cup is a titanium tube with a hollow aluminum cylinder inside it. A BNC connector is used to bias the Faraday cup with 200 volts to prevent secondary electron emission.

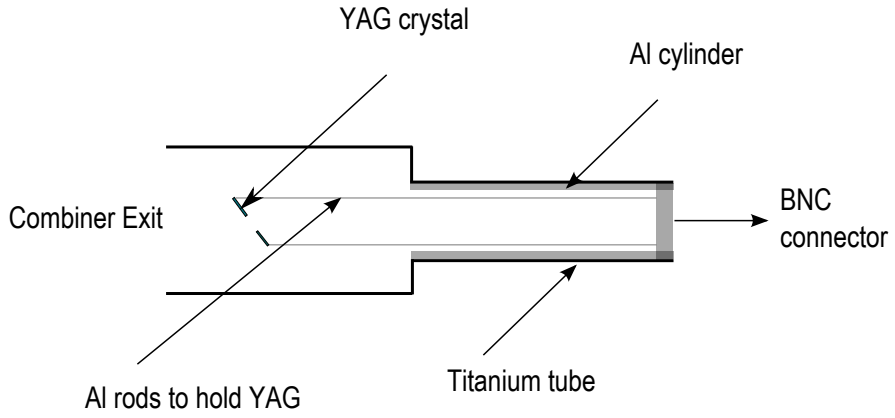

Figure 3.16: Schematic diagram of the YAG crystal and Faraday cup section

3.2.5 Vacuum components

The various vacuum components on the gun is listed in Table 3.3. To achieve low 10^{-11} Torr scale vacuum, the gun assembly was baked at 120-150 ^{0}C for 2 weeks. The vacuum in the gun is measured by a commercially available ULVAC Axtran XHV gauge. A SRS residual gas analyser can measure the partial pressures of different gas species at the back of the gun vessel. The lowest measured vacuum in the gun assembly is 2.1×10^{-11} Torr.

Pump type	Location	Pumping speed
Ion pump	Cathode loading chamber	100 l/s
TSP ×3	HV vessel	6000 l/s
Ion pump + TSP	Bottom of HV vessel	3200 l/s
Ion pump + TSP	Bottom of anode assembly	3200 l/s

Table 3.3: Vacuum pumps in the gun assembly

3.3 High voltage conditioning process

After the gun has reached its ultimate pressure, it was high voltage conditioned. This process is intended to get rid of any field emitters that might be present in the high voltage section of the gun. Low level field emission can create unwanted gas load which is detrimental to the cathode lifetime (refer to section 2.3).

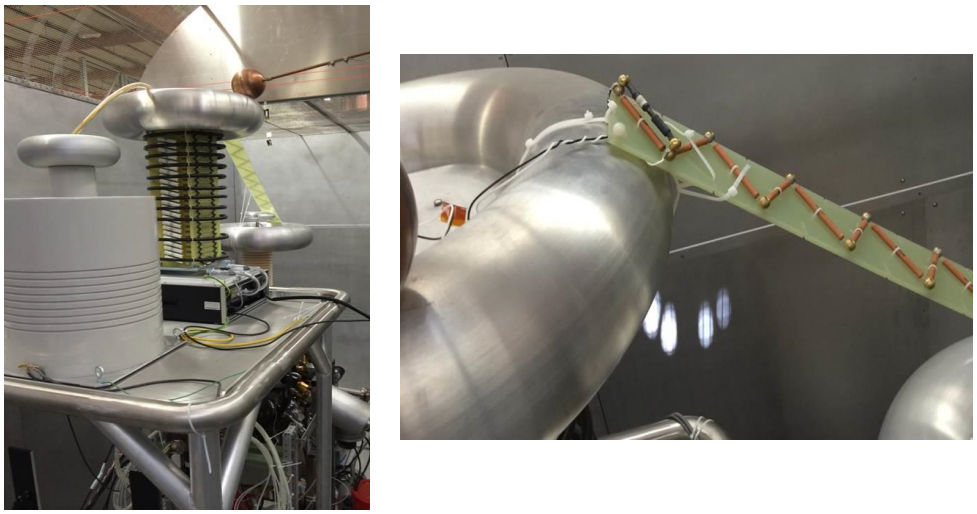

Figure 3.17: Left: High voltage power supply with the corona ring and isolation transformer to provide power to beam instrumentation. Right: Series resistor connection to protect the gun from arcing.

A -250 KV Glassman power supply was used as the high voltage source. A 90 MΩ resistor was connected in series between the power supply and the gun. This resistor acts as a protective measure as a negative feedback; the higher the current in the gun, the higher the voltage drop across this resistor and the lower the voltage across the DC gap. This limits the maximum current of the gun to 2.78 mA for 250 KV. It is important to limit the current during high voltage conditioning because a high peak current discharge can deposit a lot of power in a small spot and can damage the DC gap. A smaller resistor of 9 KΩ was in series with the 90 MΩ resistor. A fiber coupled analog link, AFL 300, was used to measure the voltage across the 9 KΩ resistor to calculate the current through the DC gap. Radiation detectors were placed at a radial configuration around the DC gap to pick up radiation from field emission. Vacuum gauge reading and ion pump current excursions were also monitored.

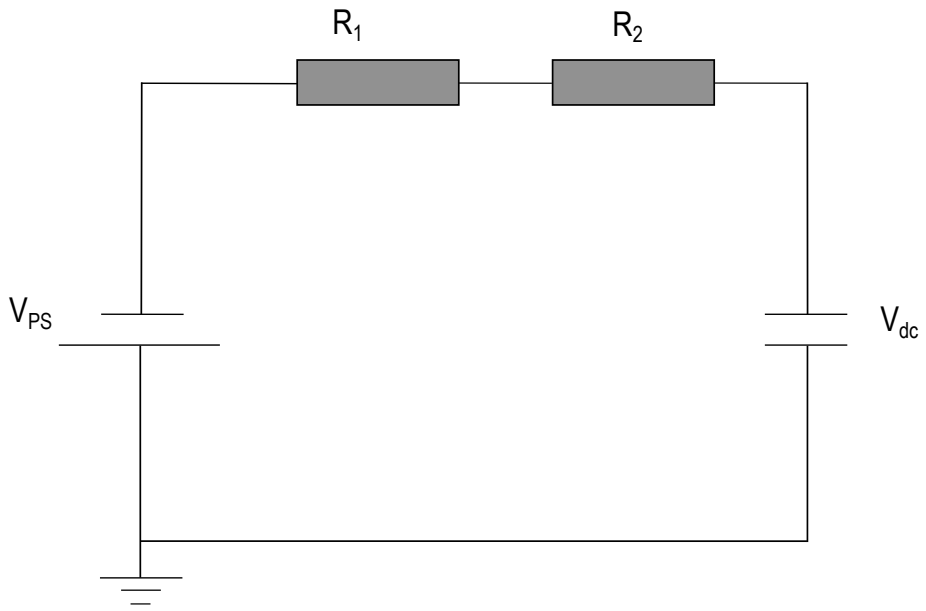

Figure 3.18: Resistor network in series to limit the current in the DC gap. R_1 is a 9 KΩ resistor and R_2 is 90 MΩ. Current through the DC gap is measured by measuring the voltage across R_1.

The high voltage conditioning was performed in two vacuum configuration. The first set of conditioning was done with gun system at 10^{-11} Torr vacuum level. For the second conditioning, the gun assembly was backfilled with ultra

high purity krypton to 1×10^{-6} Torr. Experience from CEBAF and experiments performed at JLab suggested that a protective gas such as krypton can condition faster[51].

For conditioning the gun, the voltage on the power supply was increased gradually while monitoring the current. Once the current started to increase, the voltage was increased such that the total power in the gun was less than 2 W. The power supply software control had a current limit for power supply trip. After reaching a barrier, the idea was to increase the voltage for 1-2 W power without triggering the software trip limit. Geiger counters around the high voltage area showed radiation counts corresponding to the increased field emission current. The voltage was kept constant until the current and radiation values drop to background level. Figure 3.19 and 3.20 shows typical field emitter characteristics during conditioning.

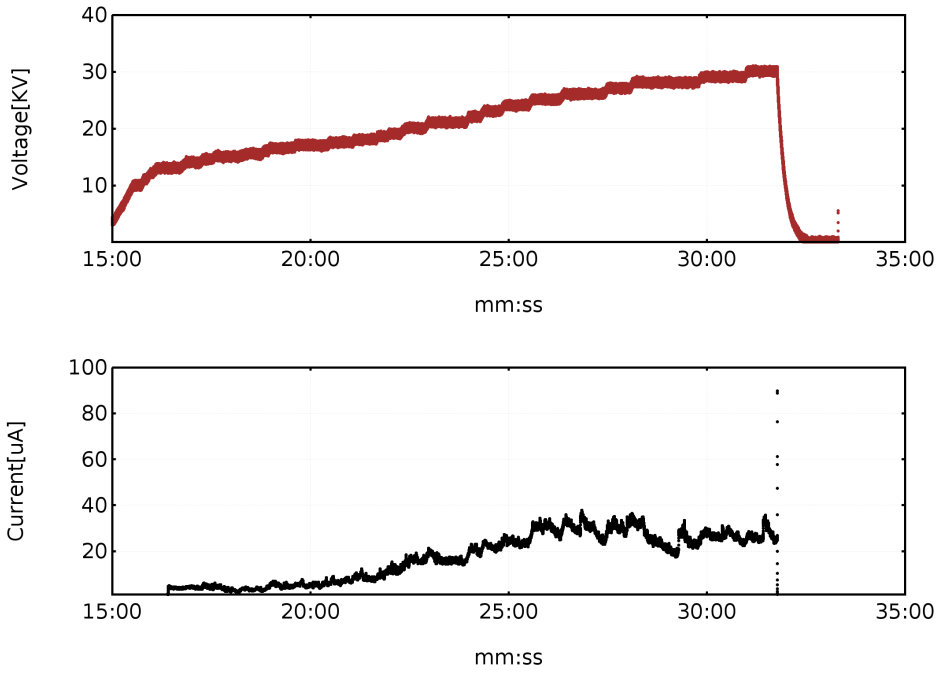

Figure 3.19: High voltage conditioning of the gun on September 25th at 16:00. The current increased exponentially at around 12 KV voltage indicating a field emitter. The current drops to zero with a subsequent power supply trip triggered by the control software current limit. The power supply trip is triggered when the current reached the software trip limit. For this particular case, it was set to 100 μA.

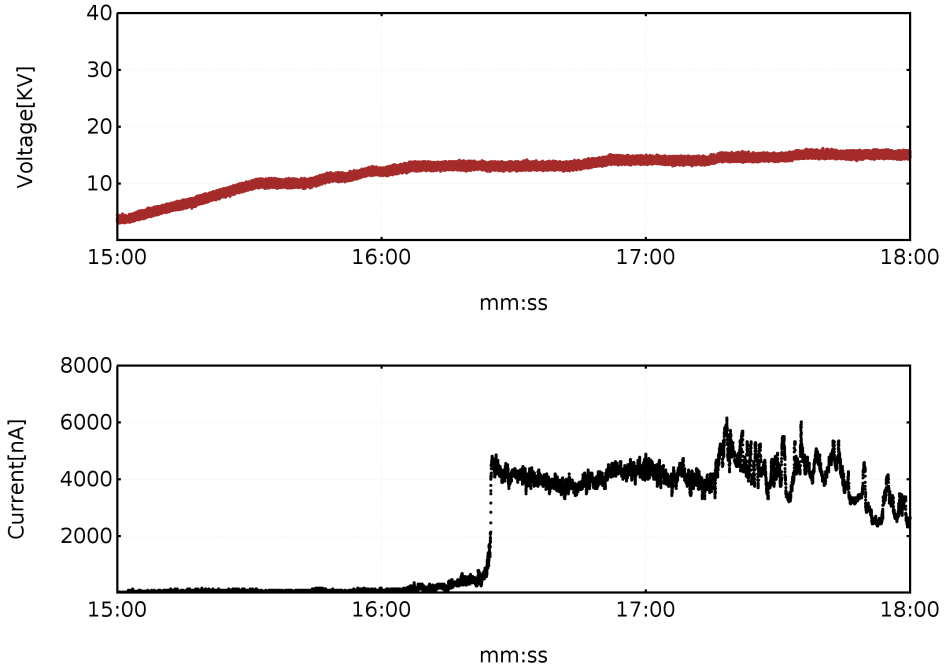

Figure 3.20: Zoomed in version of the field emitter shown in figure 3.19. The current increased exponentially with voltage at 12 KV, indicating field emission current.

The gun was high voltage conditioned under 10^{-11} Torr vacuum for a month between August 20, 2015 and September 25, 2015. The maximum achievable voltage during this period was 55 KV. Multiple field emitters around 17 KV and 35 KV were conditioned away during this time. A timeline of the high voltage conditioning history of the gun is listed in table 3.4.

High voltage conditioning under vacuum showed slow progress. After conditioning the gun for 200 hours over a month, the maximum achievable voltage without field emission was 34 KV. Figure 3.21 shows a typical conditioning process under 10^{-11} Torr vacuum. High voltage conditioning for DC guns at Jlab has shown faster conditioning by using a protective gas as krypton [51]. The electrons from the field emitter can ionize the heavy Krypton molecules and the positive Krypton ions can sputter away field emitter. To backfill the gun assembly with Kr, a leak valve on the main gun vessel was used. A steady Kr pressure of $1\times\ 10^{-6}$ Torr was achieved by controlling the leak rate and throttling the turbo pump. All ion pumps were turned off. A residual gas analyzer was used to measure the partial pressure of Kr.

Date	Starting Voltage	Final Voltage
Aug. 14 – Aug. 20	17 KV	34 KV
Aug. 21 – Sep 8	35 KV	17 KV
Sep. 10 – Sep. 11	17 KV	53 KV
Sep. 14 – Sep. 20	17 KV	34 KV

Table 3.4: High voltage conditioning during August-September 2015. 'Starting Voltage' corresponds to the voltage for the first field emitter during that period. 'Final Voltage' corresponds to the last.

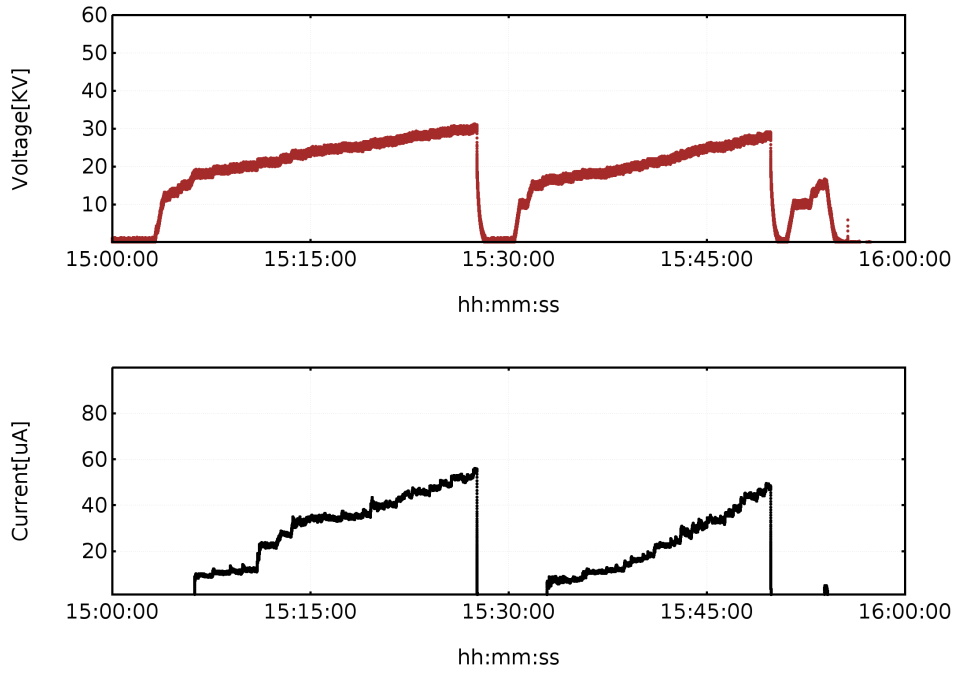

Figure 3.21: High voltage conditioning in 10^{-11} Torr vacuum during September 25, 2015. Field emission onset is at 12–15 KV and the power supply software trip is triggered at 32 KV. The field emitter is not conditioned away after two attempts.

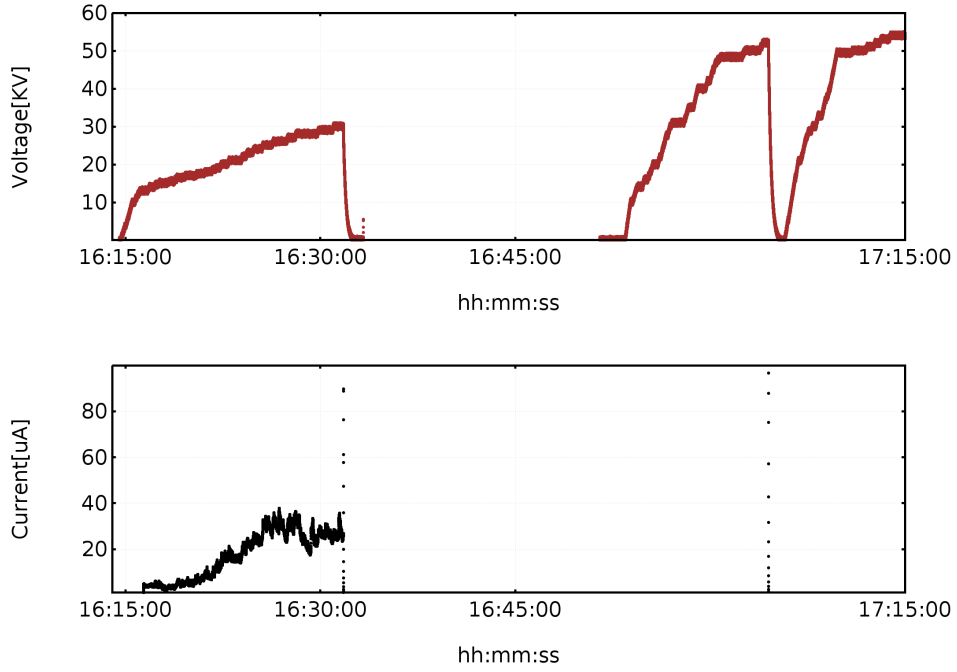

Figure 3.22: High voltage conditioning with 1×10^{-6} Torr Kr pressure during September 25, 2015. The field emitter at 12 KV is conditioned away triggering a power supply trip due to the software trip limit. Later in the hour, voltage was increased to 55 KV and no field emission current was seen.

Krypton conditioning yielded much better results in terms of achieving a higher voltage in a short period of time. Figure 3.22 shows the krypton conditioning process during September 25, 2015. The field emitter at 12 KV was conditioned in 30 minutes. The voltage was increased to 55 KV without any measurable current.

After Kr conditioning was finished, the leak valve was closed and the Kr was pumped out by the turbo pump. Once the vacuum reached low 10^{-10} Torr, ion pumps were turned back on and the turbo was valved off. Within the next 2 hours, the gun assembly reached the ultimate vacuum of low 10^{-11} Torr. At this point, the gun was field emitter free up to 55 KV.

The gun vacuum chamber was opened in order to modify the location of the YAG crystal, meaning the gun was bled up to atmospheric pressure with boil-off N_2. The system went under the bakeout procedure to obtain the ultimate vacuum of low 10^{-11} Torr. The gun was conditioned once again, first under vacuum and then under Kr.

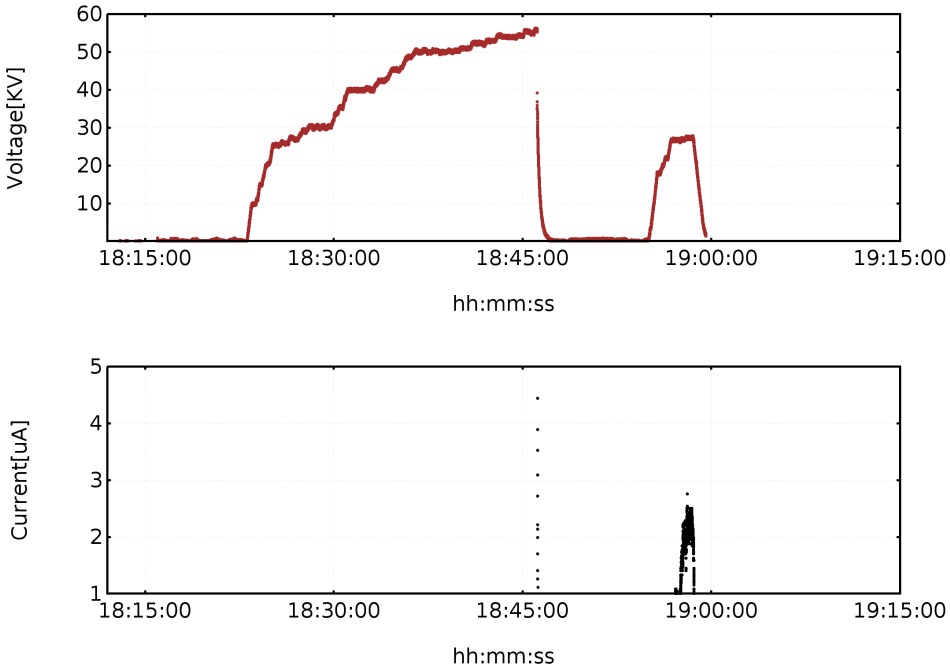

Figure 3.23: High voltage conditioning under 10^{-11} Torr vacuum on January 12, 2016. The gun could hold up to 55 KV, before power supply tripped. After the power supply trip, 27 KV was found to have a field emitter. The vacuum conditioning was then stopped to proceed with Kr conditioning.

The purpose of the high voltage conditioning under vacuum on January 16, 2016 was to verify if the gun 'remembers' the previous conditioning. At the first attempt, gun voltage was raised up to 55 KV. A sudden field emitter at 55 KV caused a power supply trip and after restarting, the field emitter onset was found to be 27 KV. It is not unusual for the field emitter onset voltage to be lower after first trip. This phenomena was also observed during August–September 2015 conditioning process and also from Jlab high voltage conditioning experience. During high voltage conditioning, the microscopic protrusions are conditioned away by localized overheating due to current flow [52]. The emitter then explodes, which can either flatten the protrusion or create a sharper protrusion with a lower field emitting onset. This explains the onset lowering from 55 KV to 27 KV after the power supply trip.

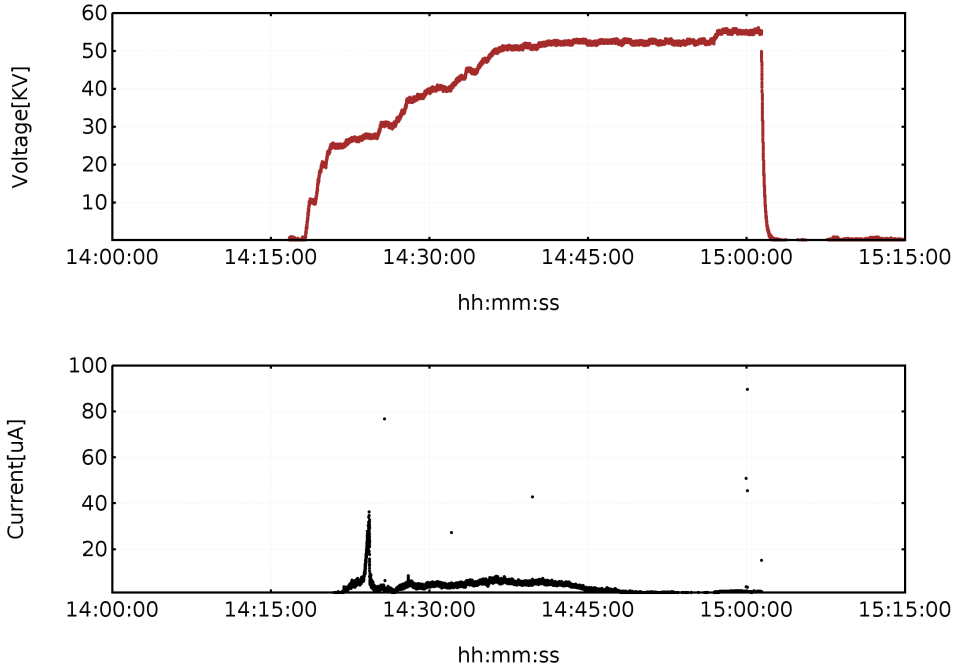

Figure 3.24: High voltage conditioning with 1×10^{-6} Torr Kr pressure. The field emitter was conditioned away after an hour of Kr conditioning.

Since Kr conditioning yields much faster results from our previous experience, the gun was Kr conditioned on January 13, 2016. As shown in figure 3.24, the 27 KV field emitter was conditioned away in 15 minutes. In an hour, the voltage was increased to 55 KV without any field emitters.

3.4 Summary

In this chapter, we described the experimental setup for two beam combination test. The mechanical and vacuum design of the cathode preparation system and the transfer line were discussed. High temperature bakeout procedure, cathode activation methods and results were presented. The preparation chamber is shown to have good vacuum performance required for cathode activation. The QE values are acceptable for the cathodes to be tested in the gun. The gun design was presented including the mechanical design of various components, the beam optics and the Faraday cup section. The final section was dedicated for high voltage conditioning and performance of the gun. The gun was conditioned extensively to eliminate any field emission for voltages below 55 KV. The vacuum performance of the gun was shown to be accept-

able for GaAs operation. Activated cathodes with good QE, good vacuum in the gun system and no field emission in the gun are essential for a two beam combination test. This chapter describes all the components on the essentials check-list for a meaningful measurement of charge lifetime from two beam combination test.

Chapter 4

Beam Test: Results and Discussion

4.1 Theory and beam funneling scheme

The ion back bombardment related decay of photocurrent from a GaAs cathode, for a constant laser power, can be written as

$$I(t) = I_0 \times e^{-t/\tau_{ibb}} \tag{4.1}$$

where, I_0 is the initial current and τ_{ibb} is the time constant of decay due to ion back bombardment (IBB). The charge lifetime due to ion back bombardment can be obtained by integrating the current as

$$Q = \int_0^\infty I(t)dt = I_0\tau_{ibb} \tag{4.2}$$

Grames et al.[15] have shown that if ion back bombardment is the only factor contributing to the decay of current, charge lifetime per unit area is a constant for a gun operating under same operating condition. In other words, if the laser spot size is fixed for a gun, the charge lifetime, Q_{ibb}, is a constant. The choice of I_0 should not affect Q because τ_{ibb} will have a value for a specific I_0 such that Q is always constant.

Consider two separate single cathode guns with charge lifetimes Q_1 and Q_2. If the beams from the guns can be combined such that the funneling does not affect the charge lifetime of individual cathodes, then the charge lifetime after funneling should be $Q_1 + Q_2$. Our goal is to demonstrate that the total charge lifetime after funneling two beams is $Q_1 + Q_2$.

For a specific average current I_1 and IBB lifetime τ_{ibb1}, the charge lifetime Q_1 is $I_1\tau_{ibb1}$. Similarly for the second gun, the charge lifetime can be written as $I_2\tau_{ibb2}$. If the average current during funneling is I_c, then we have to show – using two beam funneling test – that

$$I_1\tau_1 + I_2\tau_2 = I_c\tau_{ibb12} \tag{4.3}$$

Where τ_{ibb12} is the IBB lifetime of the source during beam funneling operation. If $I_1 = I_2 = I_0$, equation 4.3 becomes

$$I_0(\tau_{ibb1} + \tau_{ibb2}) = I_c\tau_{ibb12} \tag{4.4}$$

Depending on the value of I_c, a relationship between τ_{ibb1}, τ_{ibb2} and τ_{ibb12} can be established. For example: if we chose $I_c = 2I_0$ after beam funneling, then from equation 4.4,

$$\tau_{ibb1} + \tau_{ibb2} = 2\tau_{ibb12} \tag{4.5}$$

In our particular case, we chose $I_c = I_0$, which simplifies equation 4.3 to

$$\tau_{ibb1} + \tau_{ibb2} = \tau_{ibb12} \tag{4.6}$$

Equation 4.6 means that, if the IBB lifetime for two beam funneling is the sum of the individual cathode IBB lifetime for the same average current, the charge lifetime for two beam funneling was $Q_1 + Q_2$. Therefore,by measuring τ_{ibb1}, τ_{ibb2} and τ_{ibb12} from the experiment for a specific I_0, we can verify equation 4.3.

During beam operation, the measured decay time directly from current decay with time is the operational lifetime (τ_{op}). The operational lifetime includes contributions from different lifetime limiting factors including IBB. Therefore, we will have to extract IBB lifetimes from directly measured operational lifetimes. In section 2.3, we discussed various limiting effects on GaAs lifetime during cathode operation. Each of these effects can be assigned a respective lifetime measured in units of time. For example: background lifetime (τ_b) is defined as the time as the during which QE drops to $1/e$ of its initial value and can be measured in the gun without continuous beam operation. The operational lifetime of a photocathode (τ_{op}) is a measured quantity during the operation. The operational lifetime is related to the different effects that limit cathode operation lifetime as follow,

$$\frac{1}{\tau_{op}} = \frac{1}{\tau_b} + \frac{1}{\tau_{ibb}} + \frac{1}{\tau_p} + \frac{1}{\tau_{fe}} \tag{4.7}$$

Where,
τ_b = Lifetime due to background vacuum pressure.
τ_{ibb} = Lifetime due to ion back bombardment.
τ_p = Lifetime due to poisoning by outgassing produced during cathode operation.
τ_{fe} = Lifetime due to outgassing produced by field emission.

For a fixed operational condition – background vacuum, laser power, high voltage – every quantity on the right hand side of equation 4.7, except τ_{ibb}, is constant and can be written as a single "dark" lifetime, τ_d. Equation 4.7 can then be rewritten as,

$$\frac{1}{\tau_{op}} = \frac{1}{\tau_{ibb}} + \frac{1}{\tau_d} \tag{4.8}$$

Where

$$\frac{1}{\tau_d} = \frac{1}{\tau_b} + \frac{1}{\tau_p} + \frac{1}{\tau_{fe}} \tag{4.9}$$

Once τ_d and τ_{op} are measured at the experiment, τ_{ibb} can be calculated using 4.8.Using 4.8, we can write, for cathode one,

$$\frac{1}{\tau_{ibb1}} = \frac{1}{\tau_{op1}} - \frac{1}{\tau_{d1}} \tag{4.10}$$

And for cathode two,

$$\frac{1}{\tau_{ibb2}} = \frac{1}{\tau_{op2}} - \frac{1}{\tau_{d2}} \tag{4.11}$$

When both the cathodes are operational together, we can write,

$$\frac{1}{\tau_{ibb12}} = \frac{1}{\tau_{op12}} - \frac{1}{\tau_{d12}} \tag{4.12}$$

τ_{op} and τ_d for each cathodes in single mode and funneling mode can measured directly from the experiment. τ_{op} is the decay lifetime directly measured from the current decay for a fixed laser power. τ_d includes effect from background vacuum, field emission and cathode poisoning due to outgassing during operation. All these effects are vacuum dependent. The two cathodes are located in the same vacuum chamber and are exposed to the same vacuum condition. So every vacuum related effect during beam operation should affect both cathodes. Therefore to measure τ_{d1}, we measured the dark lifetime of cathode 2 when cathode 1 is in operation. Once these quantities are measured, the ion back bombardment dominated lifetimes are calculated using equation 4.10, 4.11 and 4.12 and thus, equation 4.6 can be verified.

The assumption leading to equation 4.6 is that the cathodes are separated and their operation is independent. In the funnelling gun, the cathodes are located in the same vacuum chamber and are not physically vacuum isolated. So for equation 4.6 to be true in this experimental configuration, the vacuum level should be the same in the gun chamber for both single beam and two beam operation. In the ideal experiment, both the average current and charge lifetime of the source should be doubled after two beams are combined. We found that doubling the current would change the pressure in the gun due to outgassing from the Faraday cup. For example: for 175 nA average current from any cathode, the pressure in the DC gun was stable around 2-2.2$\times 10^{-11}$ Torr. When the current is doubled to 350 nA from two cathodes, the pressure

would increase to 3.5×10^{-11} Torr. For this reason, we chose to combine the charge lifetime without doubling the current.

The tests to establish addition of charge lifetime were done in three steps. The first step was to measure a single cathode background lifetime (τ_b from equation 4.7) and CW operational lifetime. The single cathode lifetimes are benchmark measurements to understand how long the cathode might survive in the gun with or without beam. Experimental limits were also determined using a single cathode. The second step was to perform two beam funneling tests for an average current of 175 nA. Both operational lifetimes and dark lifetimes were measured for both cathodes for individual and two beam operation. The third and final step was to repeat the beam funneling test for 350 nA average current to check reproducibility of the results.

4.2 Single cathode beam test

The first set of beam tests was single cathode operation. The purpose of this test was to determine the background lifetime of the photocathode in the gun and to find the upper limit on the average current at which the gun can operate.

The background lifetime is defined as the time by which the QE of the cathode drops to $1/e$ of its initial value due to background vacuum. There is no continuous beam extraction during this measurement which means that this lifetime is only dependent on background pressure. The decay for background should be slow so that the comparatively faster ion back bombardment decay is easily noticed during beam operation. A slow background decay also means that the vacuum is good and the residual molecular density present in the DC gap is low. That means there are fewer molecules present to be ionized during beam operation to damage the cathode. Section 4.2.2 discusses the single cathode dark lifetime vacuum measurement.

Finding a range of average current at which the gun can be operated with existing equipment is also important. Starting out with a high current value can lead to outgassing from the beam stop and short lifetime values. Equipment limitations can also limit the highest average current in the gun and are discussed in section 4.2.4 and 4.2.4.

4.2.1 Test procedure

For single cathode tests, a bulk GaAs sample was activated and then transferred to the gun. The voltage was gradually increased to 45 KV. The electron beam transport optics was set for 45 KeV beam and then the laser was turned on. Optics was tuned so that most of the beam passed through the hole in the YAG and the current reading from the Faraday cup was maximized. The first test was to measure the background lifetime of the cathode. After background lifetime was measured, CW beam was extracted to obtain an operational lifetime value to compare with the background lifetime value. The final experiment with one cathode was to determine operational limit of the gun due to existing equipment. This was done by increasing the current in steps and monitoring vacuum pressure and beam stability.

4.2.2 Single Cathode background lifetime measurement

For single cathode background lifetime measurement, the initial QE of the cathode was 5.5% . The laser power was set to 15 μW. After tuning the optics, the laser was turned off and would only be on for a second every 30 minutes for 5 hours. The pressure of the gun was measured to be 2.0-2.2 $\times 10^{-11}$ Torr. Plotting the current values against time and fitting a exponential decay curve to the plot gives the background lifetime to be 190000 seconds or 52.7 hours.

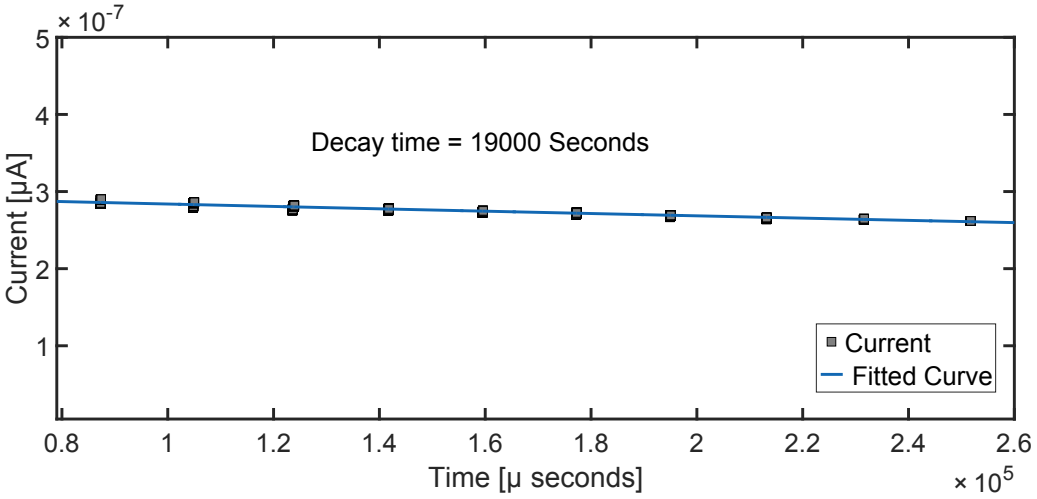

Figure 4.1: Dark lifetime measurement for single cathode at 45 KeV.

4.2.3 Single cathode CW operational lifetime measurement

After the background lifetime measurement, CW beam operation was performed to determined the CW operational lifetime for $I_0 = 300$ nA. To measure ion back bombardment dominated lifetime, a clear decay while beam operation should be observed and operational lifetime should be much lower as compared to the background lifetime. If for 300 nA, the operational lifetime is comparable to the background lifetime, the current will have to be increased in order to measure ion back bombardment induced decay. Figure 4.2 shows the CW operation curve. The pressure of the gun was measured to be 2.1-2.4 $\times$ 10^{-11} Torr. The operational lifetime is calculated to be 17500 seconds or 4.86 hours. It is much lower compared to the background lifetime of 52.7 hours which means that at 300 nA average current level, the effect of ion back bombardment can already be measured.

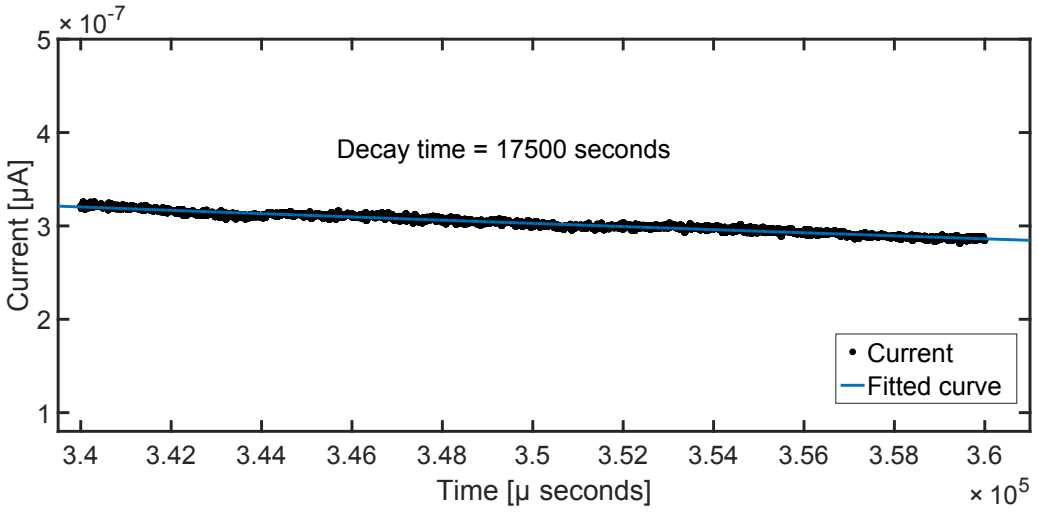

Figure 4.2: Operational lifetime in CW mode for $I_0 = 320$ nA at 45 KeV. Data was collected every 10 ms. The decay lifetime is 17500 seconds.

4.2.4 Experimental limits

After measuring the background and operational lifetime of one cathode, we determined the experimental limit of the gun system. A useful beam test requires a stable vacuum at low 10^{-11} Torr scale. The beam operation should also be stable once the optics is tuned. A straightforward way to check the experimental limit was to keep increasing the current until we found vacuum conditions unsuitable for beam operation. As the current is increased, more

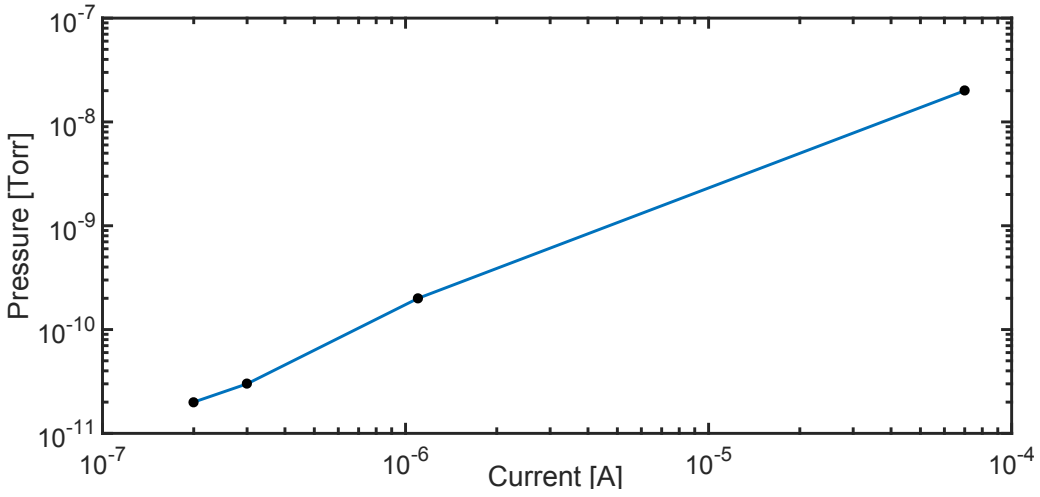

Figure 4.3: Vacuum level in the gun chamber as a function of average current. For average currents higher than 1 μA, the pressure in the gun chamber goes beyond 1×10^{-11} Torr which is not acceptable for beam operation. The gauge has a resolution of 2×10^{-12} Torr.

and more power is deposited in the Faraday cup causing outgassing. The current value at which the vacuum in the DC gap is increased to 10^{-10} Torr is the maximum average current for the existing gun equipment. While increasing the current, it was found that the ceramic vacuum tube imposes another limit on the achievable average current.

Faraday cup outgassing

In order to establish a limit at which the Faraday cup outgassing becomes dominant, we increased the laser power in steps to increase the average current. For every average current, the pressure in the gun chamber was monitored by the ULVAC Axtran gauge. The baseline pressure of the gun system during 300 nA CW operation was 2-2.4 $\times$ 10^{-11} Torr. For average currents higher than 1 μA, the pressure in the gun chamber was measured to be higher than 1×10^{-10} Torr. GaAs should be operated vacuum below 5×10^{-11} Torr to have measurable operational lifetimes. A highest current of 70 μA was driven for a short period of time since it resulted in 10^{-8} scale vacuum and killed the cathode within seconds. This limited the maximum operational limit of the average current to 1 μA.

Ceramic discharge issues

Another limiting factor towards maximum operational current was found to be ceramic discharge in the combiner magnet. During CW beam operation at currents higher than 500 nA, it was observed that the beam spot on the YAG crystal would steadily move without any change of optics. It seemed that charge was building up somewhere along the beam line and pushed the beam away due to electrostatic force. At some point, the beam would suddenly come back to its original position, implying that a discharge has happened. The higher the current, the faster the movement and subsequent discharge happened. For current lower than 400 nA, the charge accumulation was slow enough to perform one hour of operation. The only place along the beam line where charge can build up is the ceramic on the combiner section.

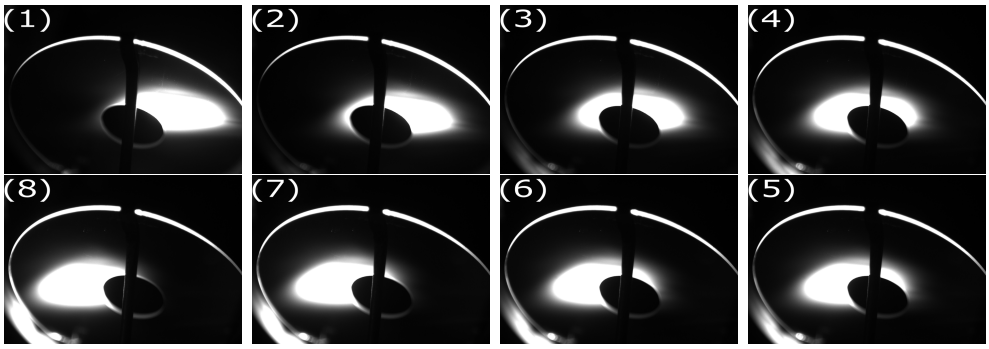

Figure 4.4: Beam spot movement as seen on the YAG crystal due to charge accumulation on the ceramic. Pictures were take 5 seconds apart for 10 μA current. Increasing figure label indicates time sequence. The beam spot was seen to move from one side of the crystal to opposite side in 40 seconds.

Recall from section 3.2.3 that the combiner magnet employs a ceramic vacuum tube as a part of the gun assembly. The inside of the ceramic tube was covered with a thin foil of Titanium to prevent charge accumulation. It is possible that during the installation and bake out of the gun, the Titanium foil might have moved exposing the ceramic body. The exposed part of the ceramic will build up charge as beam is passing close to it. The accumulated charge will cause the beam to change its trajectory. After some time, the charge will be discharged and the beam will be back to its original trajectory. Figure 4.4 shows the movement of the beam due to charge buildup on the ceramic.

The discharge was found to be very frequent for currents higher than 500 nA. Every 2-3 minutes, a discharge was observed for 1.5 μA average current.

For low current, such as 100 nA, the charge build up was slow and a discharge would only be seen after 1-1.5 hours of operation. A discharge can cause mis-steering of the beam and major outgassing from the beam pipe. This outgassing introduces instability towards the measurement of ion back bombardment lifetimes. Therefore, we decided to operate below 400 nA of average current to avoid discharge issues and have an uninterrupted measurement.

4.3 Two Cathode Beam Test

After determining the background lifetime and operation current limit of the gun, two beam funneling tests were performed. Two sets of experiments were performed with average currents 175 nA and 350 nA. The operational voltage was set to 45 KV.

4.3.1 Test procedure

Two cathodes were activated at the preparation chamber. Each cathode took about 4.5 hours to heat clean and activate. Once the first cathode was activated, it was transferred to the gun. Then the second cathode was heat cleaned and activated. The time between transfer of two cathodes is 4.5 hours. Once both cathodes were in the gun, the beam optics was tuned with low laser power and equipments were checked for proper operation. The bunch length and frequency were set for the desired duty factor. The laser power was increased for the desired average current value. First, cathode 1 was in operation whereas cathode 2 would only operate for a very short time every 10 minutes. The total operation time was 50 minutes. The procedure is then repeated for cathode 2 in operation and cathode 1 in dark. The duty factor was changed for two cathode operation mode. Two beam combining test was performed for 50 minutes. The laser power was then changed for second set of average current. The entire procedure was repeated from the start for the second set of average current.

4.3.2 Two cathode operation at 175 nA

The first set of two cathode operations were done for a starting average current of 175nA. A fresh set of photocathodes was used for this experiment. The initial QE for the cathodes in the gun were 3% and 5.28% respectively. Laser power for each cathode was adjusted to be 90 μW and 64 μW for an a peak current of 1.2 μA for both. For cathode 1 operation - cathode 2 dark test, the bunch length was set to be 330 ms and the repetition rate was 0.5 Hz. The

duty factor for individual cathode operation was 0.16. For cathode 2 operation - cathode 1 dark test, the duty factor was kept the same. For both cathode operation, the bunch length for individual cathodes were set to 165 ms. The combined frequency is 1 Hz and the duty factor for the combined current is 0.165. The pressure during beam operation was measured to be 2-2.4 $\times$ 10^{-11} Torr.

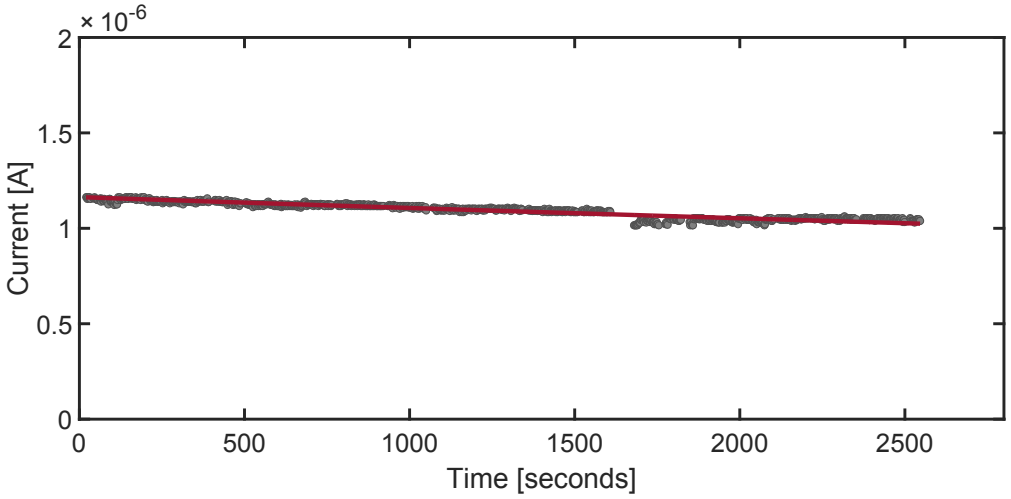

Figure 4.5: Operational lifetime measurement for cathode 1 at 0.5 Hz rep. rate and 330 ms pulse length for 175 nA average current. Data is fitted to a negative exponential with I_0= 1.16 μA and the decay lifetime is found to be 18651.6 seconds.

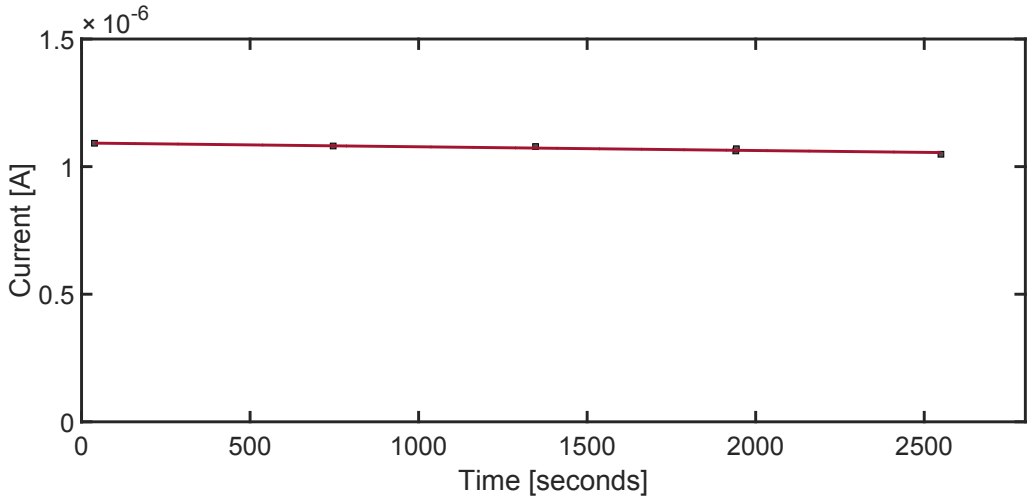

Figure 4.6: Dark lifetime measurement for cathode 2 while cathode 1 is in operation for 175 nA average current. Data was taken every 10 minutes. For I_0= 1.09 μA, the exponential decay lifetime is found to be 71600 seconds.

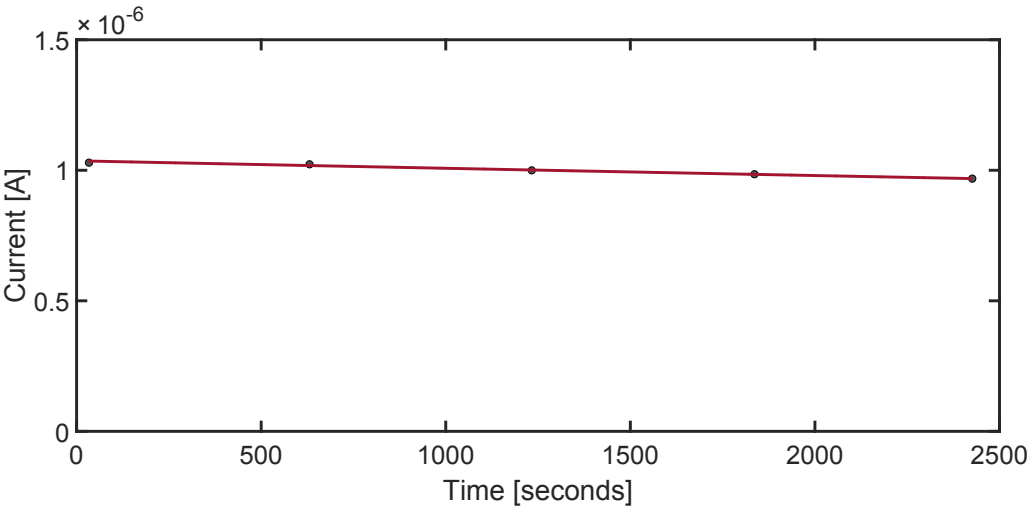

Figure 4.7: Dark lifetime measurement for cathode 1 while cathode 2 is in operation for 175 nA average current. Data was taken every 10 minutes. For I_0= 1.03 μA, the exponential decay lifetime is found to be 35697.6 seconds.

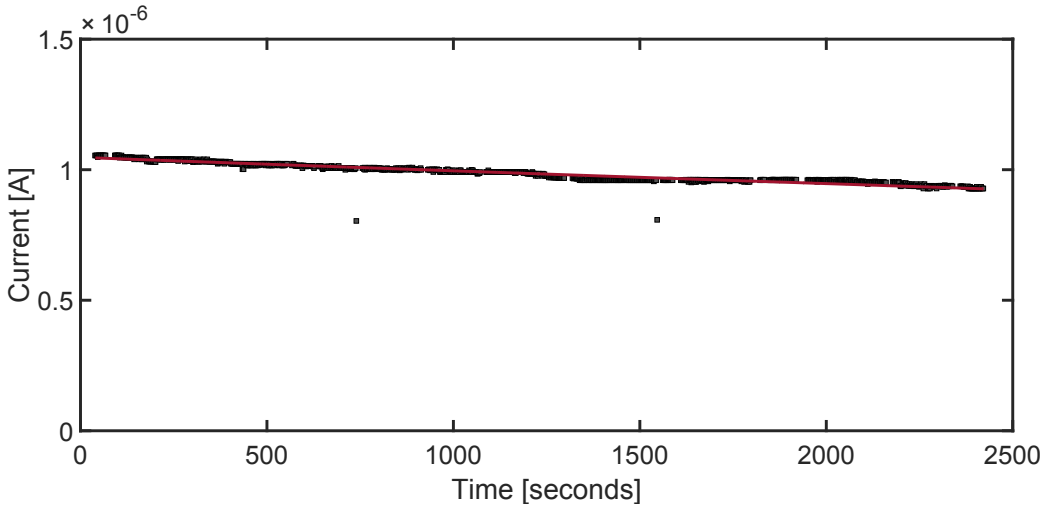

Figure 4.8: Operational lifetime measurement for cathode 2 at 0.5 Hz rep. rate and 330 ms pulse length for 175 nA average current. Data is fitted to a negative exponential with I_0= 1.047 μA and decay lifetime is found to be 18828 seconds.

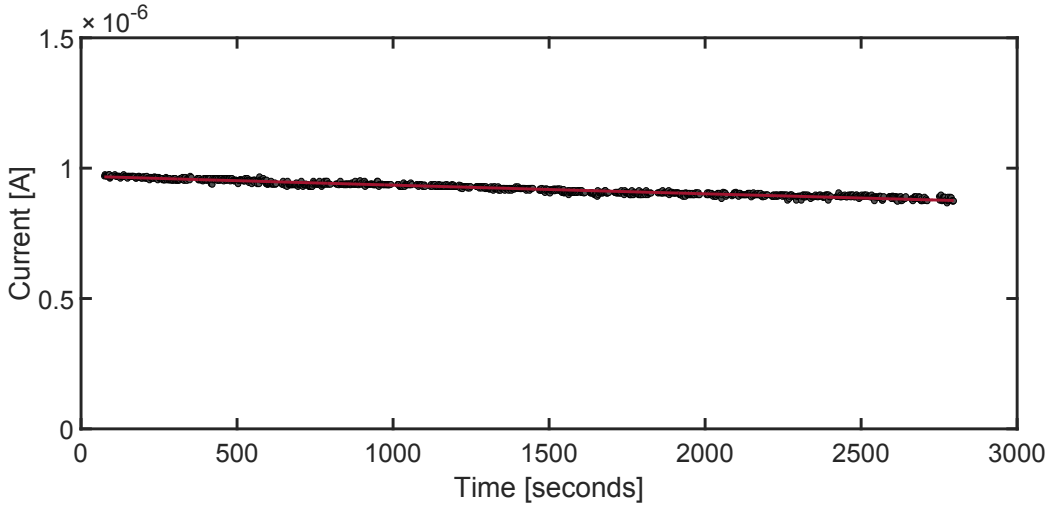

Figure 4.9: Operational lifetime measurement for cathode 1 at 0.5 Hz rep. rate and 165 ms pulse length for 175 nA average current during beam funneling run. Data is fitted to a negative exponential with I_0= 0.93 μA and the decay lifetime is found to be 27600 seconds.

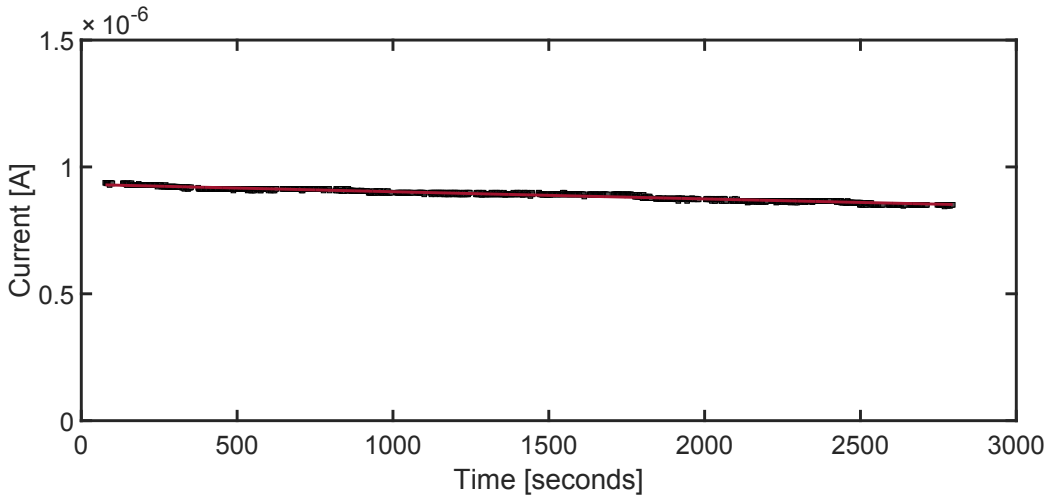

Figure 4.10: Operational lifetime measurement for cathode 2 at 0.5 Hz rep. rate and 165 ms pulse length for 175 nA average current during beam funneling run. Data is fitted to a negative exponential with I_0= 0.94 μA and the decay lifetime is found to be 31300 seconds.

4.3.3 Two cathode operation at 350 nA

For 350 nA average current tests, the starting QE for the cathodes were 1.16% and 2.66% respectively. Laser power for each cathode was adjusted to be 110 μW and 61μW for a peak current of 3 μA for both. The repetition rate was 0.5 Hz. The duty factor values were the same as 175 nA beam test. During this test, the ceramic discharge was seen during cathode 1 operation. The charge accumulation during beam test would move the beam spot on the YAG and continuous optics tuning was necessary to have the beam on the right trajectory. After a discharge, the laser was turned off for a few seconds for the vacuum to recover from beam mis-steering. After the vacuum recovered, the laser was turned back on with beam optics set-points set to the starting values of this experiment. The pressure during beam test was monitored to be 3.2-3.5 $\times$ 10^{-11} Torr.

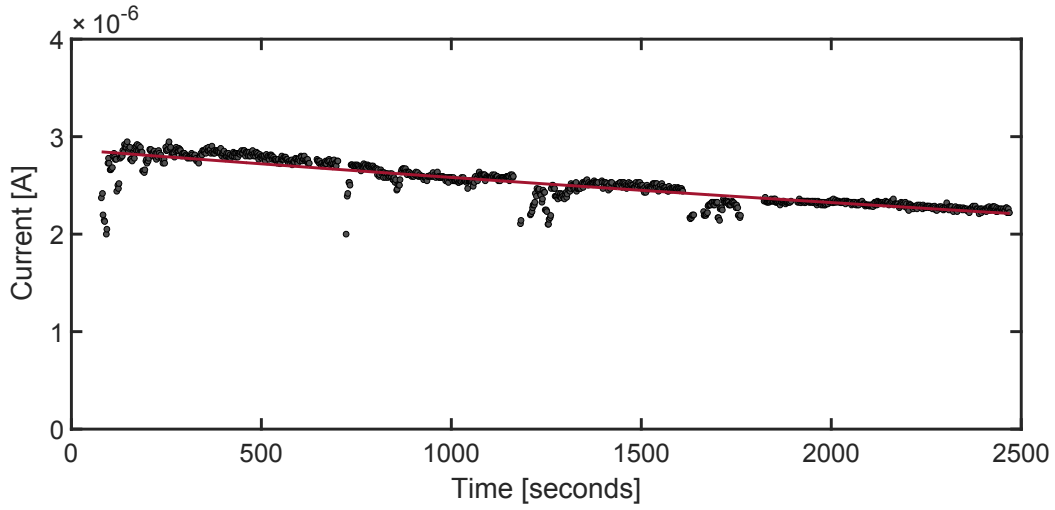

Figure 4.11: Operational lifetime measurement for cathode 1 at 0.5 Hz rep. rate and 330 ms pulse length for 350 nA average current. Data is fitted to a negative exponential with I_0= 2.89 μA and the decay lifetime is found to be 8956.8 seconds. Discontinuation on the graph is due to ceramic discharge during which laser was turned off.

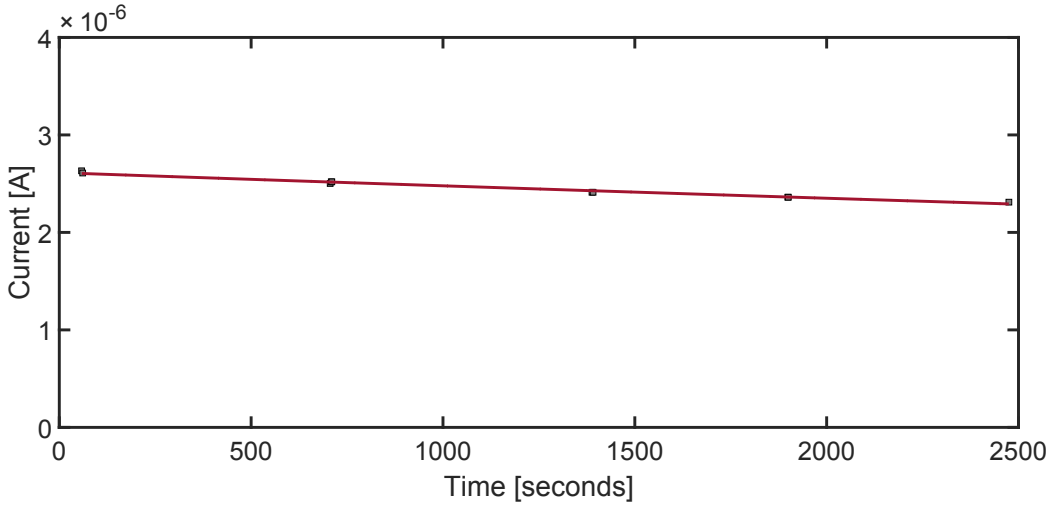

Figure 4.12: Dark lifetime measurement for cathode 2 while cathode 1 is in operation for 350 nA average current. Data was taken every 10 minutes. For I_0= 2.62 μA, the exponential decay lifetime is found to be 18972 seconds.

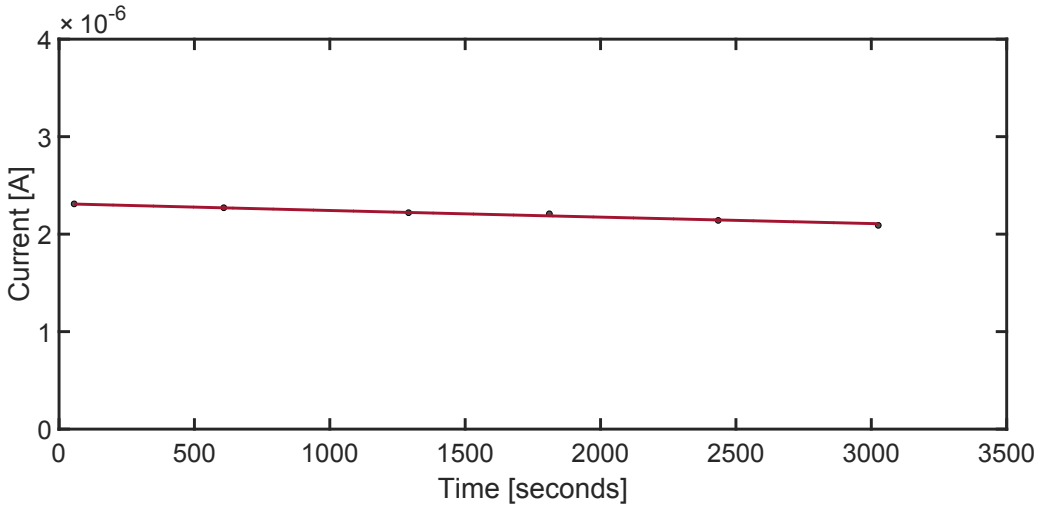

Figure 4.13: Dark lifetime measurement for cathode 1 while cathode 2 is in operation for 350 nA average current. Data was taken every 10 minutes. For I_0= 2.32 μA, the exponential decay lifetime is found to be 35700 seconds.

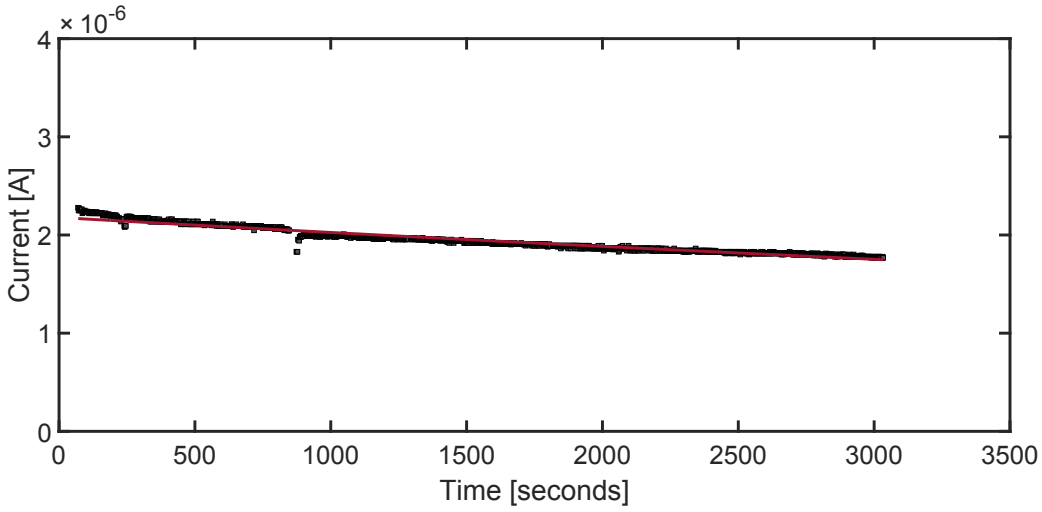

Figure 4.14: Operational lifetime measurement for cathode 2 at 0.5 Hz rep. rate and 330 ms pulse length for 350 nA average current. Data is fitted to a negative exponential with I_0= 2.23 μA and the decay lifetime is found to be 10739 seconds.

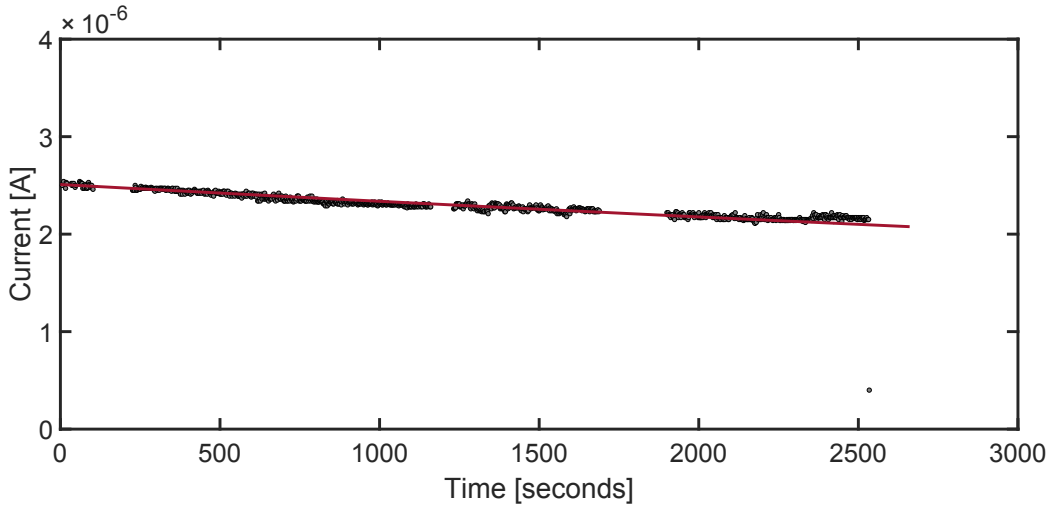

Figure 4.15: Operational lifetime measurement for cathode 1 at 0.5 Hz rep. rate and 165 ms pulse length for 350 nA average current during beam funneling run. Data is fitted to a negative exponential with I_0= 2.52 μA and decay lifetime is found to be 14400 seconds. The discontinuity in the data is due to ceramic discharge during which laser was turned off.

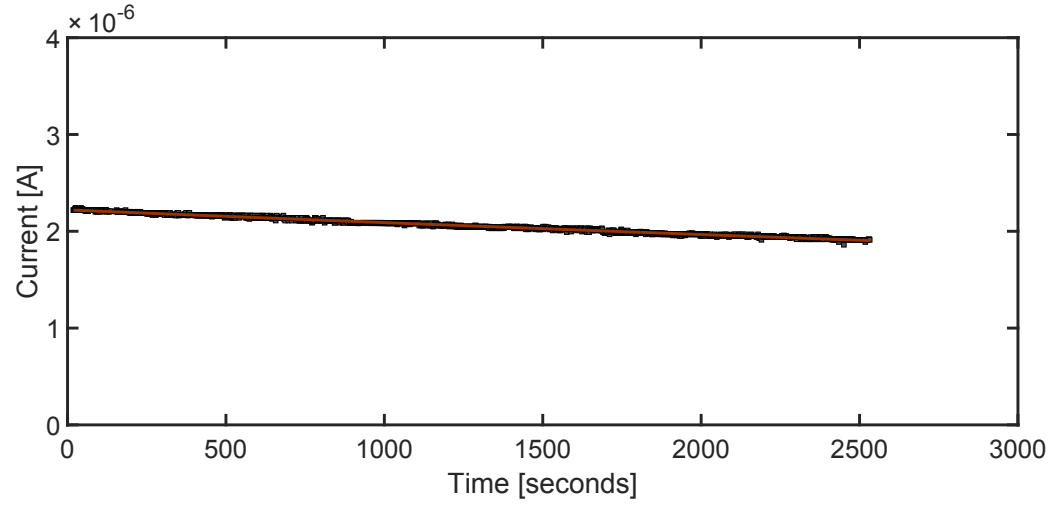

Figure 4.16: Operational lifetime measurement for cathode 2 at 0.5 Hz rep. rate and 165 ms pulse length for 175 nA average current during beam funneling run. Data is fitted to a negative exponential with I_0= 2.22 μA and the decay lifetime is found to be 16100 seconds.

4.4 Ion back bombardment dominated lifetimes

The single cathode operation results from section 4.3 is compiled into the table 4.1

Average current	τ_{op1}	τ_{op2}	τ_{d1}	τ_{d2}
nA	Hours	Hours	Hours	Hours
175	5.02 ± 0.65	5.42 ± 0.73	20.69 ± 2.5	11.26 ± 1.5
350	2.48 ±.08	2.983 ± 0.127	9.916 ± 0.298	5.27 ± 1.11

Table 4.1: Summary of 175 nA and 350 nA single cathode operation beam test results

Using the dark lifetime (τ_d) and operational lifetime (τ_{op}) values listed on table 4.1, the ion back bombardment dominated lifetimes (τ_{ibb}) can be calculated using equation 4.10 and equation 4.11 for cathode 1 and 2 respectively. Calculated values of τ_{ibb} are compiled into table 4.2. The uncertainty of each measurement was calculated by propagating the current measurement uncertainty. This is a measurement limitation due to the resolution of the scope measuring the current.

Average current	τ_{ibb1}	τ_{ibb2}	$\tau_{ibb1}+ \tau_{ibb2}$
nA	Hours	Hours	Hours
175	7.007 ± 0.97	11.067 ± 2.77	18.074 ± 2.93
350	3.321 ± 0.015	6.873 ± 2.09	10.195 ± 2.09

Table 4.2: Calculated values of ion back bombardment dominated lifetimes during single cathode operation.

For the two cathode operation experiment, the average of the operational lifetimes of cathode 1 and 2 was taken to determine the average operational lifetime ,τ_{op12}, of the gun. The reasoning behind this can be explained as following: if Q_{12} is the total charge extracted during two cathode operation, then it can be written as,

$$Q_{12} = I_1 \times \tau_1 + I_2 \times \tau_2 \tag{4.13}$$

Where,
I_1 = Initial current from cathode 1.
τ_1 = Lifetime of cathode 1.
I_2 = Initial current from cathode 2.
τ_2 = Lifetime of cathode 2.

In our case, $I_1 = I_2 = \frac{I_0}{2}$. In that case equation 4.13 can be rewritten as,

$$Q_{12} = I_0 \times (\tau_1 + \tau_2)/2 \tag{4.14}$$

Comparing equations 4.13 and 4.14, it is clear that the lifetimes for individual cathodes needs to be averaged for two beam test to obtain the average lifetime of the gun.

Since both the cathodes are in operation during this test, the dark lifetime was the average of dark lifetimes of cathode 1 and 2 from the single cathode operation tests for respective average currents.

Average current	τ_{op12}	τ_{d12}
nA	Hours	Hours
175	8.177 ± 1.335	14.898 ± 1.45
350	4.236 ± 0.22	7.593 ± 1.14

Table 4.3: Summary of 175 nA and 350 nA two cathode operation beam test results

Using equation 4.12, the ion back bombardment dominated lifetime values for the two beam funneling runs are calculated and listed in table 4.4. The sum of individual τ_{ibb}'s are listed for comparison.

Average current	τ_{ibb12}	$\tau_{ibb1} + \tau_{ibb2}$
nA	Hours	Hours
175	18.125 ± 3.6	18.074 ± 2.93
350	9.581 ± 2.084	10.195 ± 2.09

Table 4.4: Summary of 175 nA and 350 nA two cathode operation beam test results

From table 4.4, we see that the sum of ion back bombardment dominated

lifetimes for individual cathodes equals the ion back bombardment dominated lifetime during two beam operation within the experimental uncertainty. 20 nA resolution of the current measuring scope introduced a measurement uncertainty. This uncertainty was propagated in calculating the uncertainties of different τ's. Another source of experimental uncertainty was due to the inequality of I_0 values between individual and funneling beam tests. I_0 values for cathode 1 and 2 were different during single beam and two beam operation for both runs. For equation 4.6 to be true, the I_0 should be the same. The I_0 values could not be adjusted due to lack of remote control capabilities of the laser. The tests could not be interrupted because that might have changed the operating conditions. The difference in I_0 values were more during 350 nA than 175 nA, which is reflected in their uncertainty calculation.

At this point, the ion back bombardment charge lifetimes for each cathode can be calculated using their respective I_0 and τ_{ibb} values. We denote Q_1 as cathode 1 charge lifetime, Q_2 as cathode two charge lifetime and Q_{12} as the combination charge lifetime. The charge lifetimes are listed on table 4.5.

Average current	Q_1	Q_2	$Q_1 + Q_2$	Q_{12}
nA	mC	mC	mC	mC
175	4.83 ± 0.83	6.88 ± 1.89	11.7 ± 2.074	10.1 ± 2.38
350	5.7 ± 0.24	9.1 ± 2.81	14.8 ± 2.82	13.5 ± 3.01

Table 4.5: Summary of 175 nA and 350 nA charge lifetimes.

From table 4.5, the charge lifetimes of single cathodes are shown to add up when the beams are combined. The uncertainties on charge lifetimes were calculated by using the uncertainties on τ's and initial currents.

The charge lifetimes for 175 nA and 350 nA are slightly different because the conditions – dynamic vacuum and laser spot – were slightly different for the two sets. For example: during the 175 nA test,the pressure on the system was 2.2-2.4 $\times$ 10^{-11} Torr whereas it was 3.2-3.5 $\times$ 10^{-11} Torr during 350 nA operation. However, the important thing to note here is that during the course of individual set of beam test, the operating conditions were kept the same. This ensured that the Q's for a specific average current were measured under identical conditions. Also note that the sum of individual charge lifetimes, for both average currents, is higher than the funneling run. This is because, as explained in section 4.5, the dynamic vacuum of the gun has a time dependence

that affects two beam operation differently than single cathode operation.

4.5 Dynamic vacuum of the gun

From section 4.2.2, the dark lifetime of a cathode in the gun at 45 KV voltage was found to be 52 hours. The base pressure of the system was measured to be 2-2.2× 10^{-11} Torr. During the single cathode beam tests for 175 nA and 350 nA, the pressure was measured to be 2-2.4× 10^{-11} Torr and 3.2-3.5×10^{-11} Torr. However, from table 4.1, we see that the dark lifetimes during beam operations are substantially lower compared to the dark lifetime without any beam. This is particularly puzzling because dark lifetime of a photocathode is dependent only on the pressure of the system and not on charge extraction. The pressure change in the system during beam operation was negligible compared to the drastic change of dark lifetime. This might lead to the conclusion that during two beam operation, the cathodes appear to be cross talking in such a way that beam extraction from one cathode is responsible for vacuum poisoning of the other cathode.

Since 90% of the beam is transported to the Faraday cup, a good start would be to investigate whether or not the beam stop is generating enough gas that eventually makes it way back to the photocathode. Molflow+ [53], a test particle Monte Carlo algorithm based code, was used to simulate the dynamic vacuum of the gun during the beam test. We can define outgassing rates and pumping speeds for different surfaces in the gun accordingly. Once all the outgassing rates and pumping speeds are defined, the code can be used to measure pressure on the cathode surfaces. After 12 hours of running the code, a steady state pressure for the gun can be simulated. Outgassing rates for different materials used for this simulation is listed on table 4.6.

Material	Outgassing rate [Torr.l/s.cm^2]
Stainless Steel	8× 10^{-13}
Titanium	2 × 10^{-14}
Aluminium	1 × 10^{-7}

Table 4.6: Outgassing rates of different materials used for Molflow+ simulation

In order to simulate the outgassing from the beam stop, we note that outgassing from the beam stop only occurs when beam hits the Faraday cup.

Therefore the time structure of outgassing from the beam stop should have the same time structure of the beam. Since the duty factor during beam operation was 0.165, we set an outgassing from the Faraday cup to be a pulsed outgassing with 165 ms pulse width with 1 Hz repetition rate, which is the same time structure as the beam. The pulsed outgassing structure is shown in figure 4.17. We set a pressure profile monitor at the cathode surface and evaluated the pressure evolution from bunch to bunch.

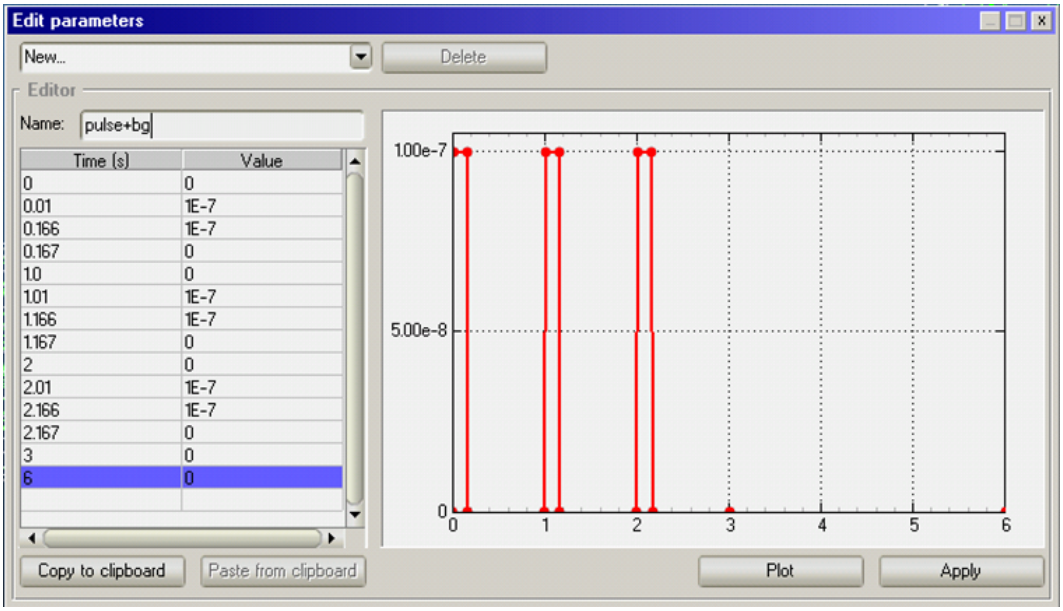

Figure 4.17: Pulsed outgassing profile from the Faraday cup. The outgassing is not continuous but pulsed corresponding to the pulsed beam structure.

The outgassing rate from the Faraday cup was chosen to be 1×10^{-7} Torr.l/s.cm^2. Since there was no experimental way to measure the outgassing rate from the Faraday cup during beam operation, this value was found from running multiple iteration of the simulation with different values of outgassing rate and picking the one that best matches the vacuum conditions during the beam test as measured from the gauge. It should also be noted that in this particular scenario, the time evolution of pressure is more revealing than the exact value of pressure. A sudden gas load due to Faraday cup outgassing from cathode 1 operation will poison cathode 2. This sudden pressure rise may not be detected at the gauge due to the position and time resolution of the gauge electronics [54]. The Molflow+ simulation of the dynamic vacuum of the gun assembly is shown in figure 4.18.

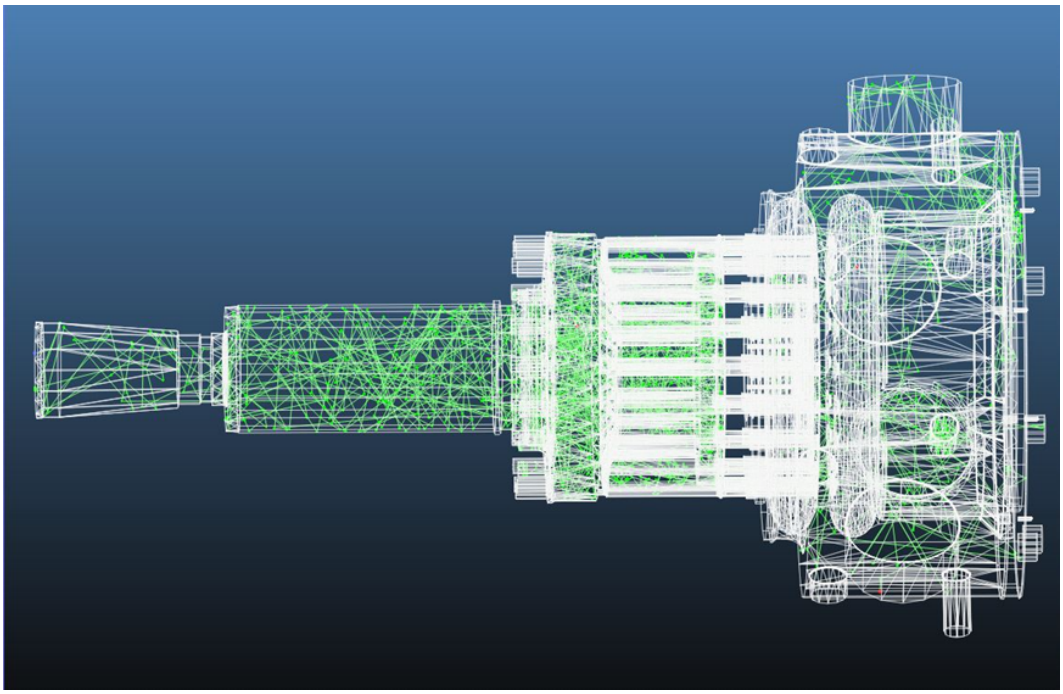

Figure 4.18: Simulation of pressure using Molflow+. The green lines show particle trajectory.

Figure 4.19 shows the pressure on the photocathode as a function of time. As the beam is stopped at the Faraday cup, the outgassing causes a pressure spike at the cathode surface. The pressure rise happens within half a second and it takes the pumps approximately 1 second to pump the gas down to baseline vacuum. This sudden rise and drop of pressure is hard to detect using a conventional Bessel box gauge due to the limitation of the time resolution of the gauge electronics.

The sudden pressure spike has a two fold effect on the photocathodes. Firstly, the pressure spike explains the lower dark lifetime of a cathode 1 during beam operation of cathode 2 and vice versa. Any gas load around the cathode poisons the cathode. Even if the pressure spike is not substantial, over the entire period of the beam operation it adds up and the dark lifetime of the cathode can decrease. During single cathode operation, this gas load only poisons the cathodes since bunch to bunch duration is 1.67 seconds.

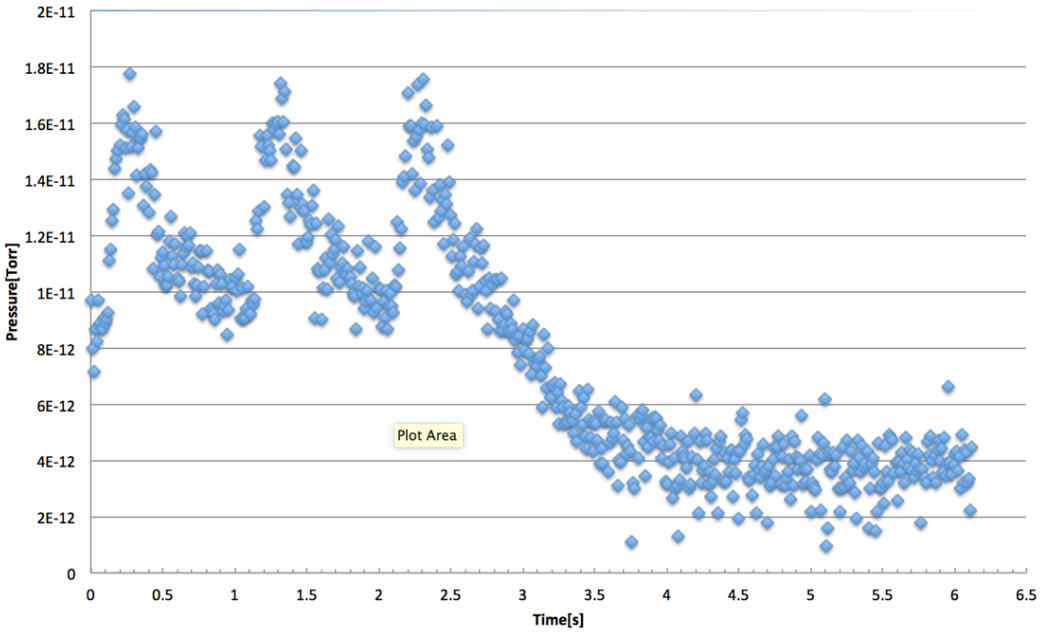

Figure 4.19: Pressure evolution on the cathode surface during beam operation

Secondly, the pumpdown of the gas load from the beam stop outgassing takes approximately 1 second. During two beam operation, the bunch to bunch duration during two beam funneling is 835 ms. After the beam pulse from cathode one has been absorbed at the Faraday cup, the vacuum at the DC gap stays elevated from the baseline pressure for approximately 1 seconds. This implies that after cathode 1 operation, cathode 2 is exposed to the gradually decreasing gas load for 835 milli seconds which is responsible for the chemical poisoning. After 835 ms, once the laser illuminates cathode 2, electrons from the cathode encounter a still decreasing gas load. Since the pressure has not recovered fully, the extra gas load contributes to the ion back bombardment damage to the cathode. Therefore the outgassing from the beam stop is not only responsible for vacuum poisoning of cathodes but also contributes to the ion back bombardment damage to the cathodes during two cathode operation. This explains why the sum of individual cathode charge lifetime is slightly higher compared to funneling charge lifetime.

The reason this gas load from the Faraday cup made it to the DC gap is because there is not enough pumping between them to intercept any gas load generated downstream. Beyond the DC gap, the gun has a 100 l/s ion pump and a 2000 l/s TSP. This amount of pumping does not seem to be

enough to maintain a stable vacuum during higher current beam test. A longer distance between the gun and the Faraday cup along with differential pumping in between can solve this issue.

4.6 Electron Hydrogen scattering in the DC gap

Another mechanism of cathode 'cross-talk' in the gun could be "Electron Simulated Desorption (ESD)". As the electrons are getting accelerated from the cathode to the anode gap, they can scatter from the residual gas molecules, change trajectory and hit the anode to produce outgassing. Naturally the scattering closest to the cathodes – in the DC gap – should contribute the most to this process. By comparing the outgassing rate from the scattered electrons to the pumping rate in the DC gap, it can be determined whether this process is significant compared to the background vacuum.

The vacuum pressure during beam test was 2×10^{-11} Torr. At this level of vacuum, the dominant gas species in the chamber is H_2. Therefore, we consider the scattering process between electrons and H_2 to determine the scattering rate. We use the total scattering cross section values (elastic and inelastic) for e-H_2 process to calculate the scattering rate.

Consider, electrons are travelling in the Z direction in a potential difference of V for a total distance of d. The expression for scattered particle rate per unit area for a given rate of incoming particle can be written as,

$$R_s = R_i \times \Phi_t \times \sigma(\varepsilon) \tag{4.15}$$

Where R_s is the scattered particles per unit time per unit area, R_i is the incoming particles per unit time per unit area, Φ_t is target particle number per unit area and $\sigma(\varepsilon)$ is total scattering cross section as a function of energy of the incoming particles.

The target particle flux is defined as the number of available target particles for the incoming beam to get scattered off. For a small increment of distance dz, the target particle density per unit area is

$$d\Phi_t = \rho_t dz \tag{4.16}$$

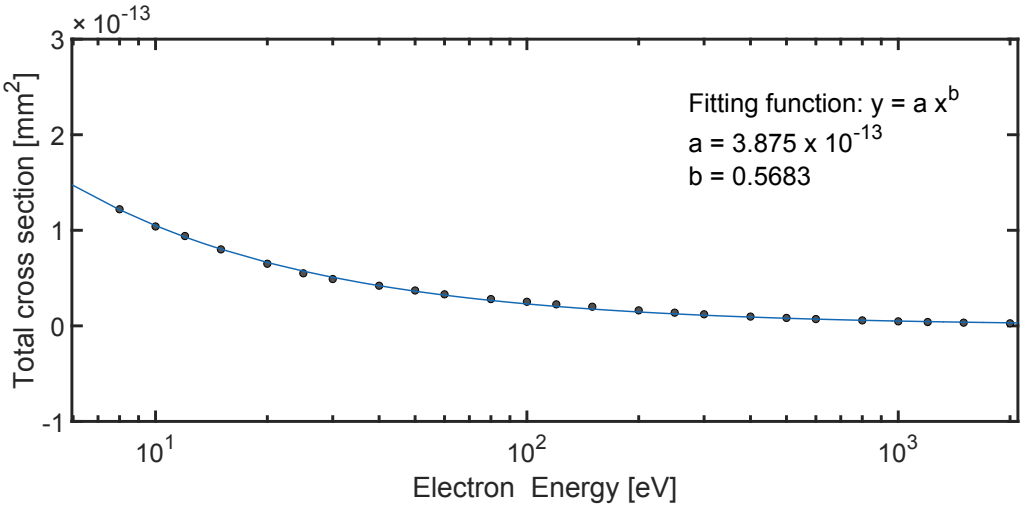

Figure 4.20: Total scattering cross section as a function of electron energy is plotted for e-H_2 process. The values used are listed on page 27 of reference [5]

.

where ρ_t is the density of target particles. Using equation 4.15, the rate of scattering for electrons travelling a distance dZ can be written as,

$$dR_s = R_i \rho_t \sigma(\varepsilon) dz \tag{4.17}$$

Total scattering cross section is a function of energy, which is a function of distance in a constant potential difference. So in principle, equation 4.17 can be integrated over z once the z dependence of $\sigma(\varepsilon)$ is known.

Scattering cross section values for e-H_2 scattering can be found in the literature [5] [55]. Cross section values for electron energies between 1 eV to 3 eV can be used from tables listed in [5]. For electron energies higher than 3 eV, a fitting curve from the tabulated values can be obtained. Figure 4.20 shows the fitting curve and the fitting function is determined to be y = ax^{-b}, where a,b are constants with values 3.875×10^{-13} and 0.5683 respectively. Equation 4.17 can be integrated over the desired limit to calculate total scattering rate.

By fitting a curve for $\sigma(\varepsilon)$ values as a function of energy (figure 4.20), we obtain that,

$$\sigma(\varepsilon) = 3.875 \times 10^{-13} \times \varepsilon^{(-0.5683)} (mm^2) \tag{4.18}$$

For an electron travelling in the Z direction in a constant electric field E,

the energy of an electron can be written as

$$\varepsilon = qVz/d = qE/z \tag{4.19}$$

Where d is gap distance. Combining equations 4.18 and 4.19, we get

$$\sigma(\varepsilon) = 3.875 \times 10^{-13} \times (qVz/d)^{(-0.5683)} \tag{4.20}$$

Plugging the value of $\sigma(\varepsilon)$ into equation 4.17, the scattering rate now can be written as

$$dR_s = R_i \times \rho_t \times 3.875 \times 10^{-13} \times (qVz/d)^{(-0.5683)} dz \tag{4.21}$$

Integrating equation 4.21 over the z values within the limit corresponding to energy values 3 eV, we can now obtain the total scattering particle rate in the DC gap for electron energies 3 eV - 45 KeV.

For this particular experiment, the various parameters on equation 4.21 are listed below:

- R_i = 4.85 $\times$ 10^{12} electrons / s.mm^2, assuming 2.5 μA current with a spot size of 3.14 mm^2.
- ρ_t = 3.3$\times 10^3$ molecules/mm^3, assuming 1$\times$ 10^{-10} Torr pressure.
- E = 1500 V/m.

The integration limit would be z values corresponding to 3 eV and 45 KeV which are .002 mm to 30 mm. Plugging all the parameters into equation 4.21 and integrating, the scattering rate of electrons per mm^2 is found to be 962 electrons. Using the tabular value of cross sections from the reference in the energy range 0.03 eV to 100 eV, R_s can be found for individual energy. Adding them all up, we get that in the energy range of 0.03eV to 3 eV, total number of particles scattered per second per mm^2 is 75. Therefore, the total number of electrons scattered in the DC gap per second per mm^2 of beam is 1051.

To be conservative, lets consider that all 1051 scattered electrons will hit the Titanium anode after passing through the DC gap. The outgassing produced from the anode can be calculated from the electron stimulated desorption yield value for Ti for 45 KeV electrons. The available literature on electron stimulated desorption yield values from Ti is limited. To estimate a realistic value for the outgassing, we chose to use electron stimulated desorption yield values from unpolished baked Stainless Steel[56]. In reality, the desorption yields for Ti will be lower than that of Stainless Steel since Ti has a much

lower outgassing rate and hence much lower concentration of trapped gas in the material.

For 45 KeV electrons, the desorption yield is found to be 0.22 molecules per electron. So 1051 electrons hitting a Stainless Steel anode will produce 231 gas molecules per second. To compare if this gas load is significant compared to background vacuum, we should compare this value with the number of molecules being pumped from the DC gap per second by the available vacuum pumps.

The gas load in the DC gap is generated from the stainless steel and titanium surfaces. In order to simplify the calculation, we consider the DC gap as a cylinder of 16 inch (0.4 m) diameter and 3 cm (.03 m) height. One circular face of this cylinder is the HV shroud which is stainless steel, the other circular face is titanium. Outgassing rate of polished stainless steel is 1.064×10^{-9} Pa.m/s. Now, outgassing from Ti = 2.66×10^{-11} Pa.m/s. So for all practical purposes, outgassing from the stainless steel is the dominant source of molecules in the DC gap. Multiplying the rate by the area of the steel shroud, we get the outgassing per second from the entire stainless steel shroud to be 1×10^{-10} Pa.m^3/s. At equilibrium, the outgassing from the walls of the chamber has to be equal to the pumping rate of the available pumps. The mass throughput from all available pumps in the chamber can be written as [57],

$$q_m = \frac{m}{t} = OutgassingRate \times \frac{M}{R \times T} \tag{4.22}$$

where

- M = Molar mass of Hydrogen molecule = 1.076×10^{-3} kg/Mole
- R = Universal Gas Constant = 8.314 J/K.Mole
- T = Temperature of the gas = room temperature = 300 K

Plugging all the values into equation 4.22, we get

$$q_m = 4.3 \times 10^{-17} kg/s \tag{4.23}$$

Dividing equation 4.23 by the mass of H_2 (1.064×10^{-27} kg), we get the total number of molecules pumped away every second to be 2.62×10^{10} molecules.

Comparing the pumping rate of 2.62×10^{10} molecules/s to the outgassing rate due to e-H_2 scattering of 2.31×10^2, we conclude that this process did not have any significant effect on cathode lifetime. This calculation can be extended further to predict if e-H_2 scattering could be a significant problem for mA operation. For example, lets consider 100 KeV electron beam with 2.5 mA average current with a laser spot size area of 3.14 mm^2. For mA level current operation, the pressure will have to be in 10^{-12} Torr scale. Using these values into equation 4.21 and integrating, 6300 electrons will be scattered per second per mm^2. If all of these electrons hit the anode, the outgassing would be 1386 molecules per second. This outgassing is still substantially lower than the pumping rate in the DC gap. So even for much higher current operation, e-H_2 in the cathode-anode gap should not be a significant factor towards lifetime decay.

4.7 Summary

In this chapter, we discussed single cathode and two cathode beam tests that were performed using the funneling gun. The "background" lifetime of a cathode in the gun was measured to be 53 hours. CW operational lifetime from single cathode was measured to be 4.86 hours. The maximum operational level for average current for the existing gun configuration was determined to be 500 nA limited by Faraday cup outgassing and combiner ceramic discharge. Two beam funneling tests for average currents 175 nA and 350 nA were performed. The average current during the beam funneling was kept to be same as the single cathode average current due to outgassing from the Faraday cup. The ion back bombardment dominated lifetimes for individual cathode operation and two beam funneling operation were measured. The charge lifetime two beam funneling operation is shown to be the sum of individual operation within the experimental uncertainties. Dynamic vacuum in the DC gap was investigated by simulation using MolFlow+. The outgassing from the Faraday cup during beam operation is found to elevate the vacuum inside the DC gap and contribute to vacuum poisoning and ion back bombardment. Outgassing created by e-H_2 scattering in the DC gap is also calculated and shown to not have a significant effect on cathode lifetime even for higher currents.

Chapter 5

Conclusion

In this dissertation, we described the construction, commissioning and two beam funneling results using a funneling gun capable of funneling 20 photocathodes to one common axis. The design and construction of the cathode preparation chamber was also described in detail. The preparation chamber is capable of achieving low 10^{-12} Torr pressure level in a consistent basis. Bulk GaAs photocathodes were activated in the preparation chamber with 6-11% quantum efficiency for 650 nm laser and then transferred to the gun for beam operation. The gun was high voltage conditioned for 48 KV and was operated at 45 KV for beam tests. The background lifetime of an activated cathode in the gun was measured to be 52 hours. Faraday cup outgassing and ceramic discharge in the gun limited the maximum average current to 400 nA for existing gun configuration. Two beam funneling tests for average currents 175 nA and 350 nA were performed and show that the charge lifetime of two beam funneling is the sum of individual cathode charge lifetimes within experimental limits.

The addition of charge lifetimes can be useful while trying to build high average current source for future electron ion collider. Short charge lifetimes from high average current polarized sources makes them unfeasible for practical collider design. 4 mA current from Jlab gun test stand yielded 80 C of charge with 5.5 hours of operation. For higher current the lifetime should be even shorter. It is impractical to change cathodes every hour for a source to be used in a collider. However the results of addition of charge lifetime can be implemented to design a more practical source. 10 identical guns with 80 C charge lifetime should give a total of 800 C charge lifetime when combined. The 800 C charge can be extracted by any choice of combined average current. If the desired average current is 20 mA, then each gun can be operated at 2 mA for 11 hours. If the desired current is 40 mA, the 80 C can be extracted from each gun at 4 mA for 5.5 hours. Therefore, beam funneling is shown to have a significant advantage over single cathode gun for high average current operation.

The experimental configuration in dissertation also shows that two cathodes can be operated in the same vacuum chamber to combine the charge lifetime. This means that under suitable conditions, two cathodes in the same chamber behaves as if their operation is independent. This result can be used to build a beam funneling scheme based electron source without building individual guns with individual gun chambers and such.

Bibliography

[1] E. J. Riehn, "Photokathoden mit internem dbr-reflektor als quellen hochintensiver spinpolarisierter elektronenstrahlen," *Diss., Universität Mainz*, 2011.

[2] J. Blakemore, "Semiconducting and other major properties of gallium arsenide," *Journal of Applied Physics*, vol. 53, no. 10, pp. R123–R181, 1982.

[3] D. T. Pierce and F. Meier, "Photoemission of spin-polarized electrons from gaas," *Physical Review B*, vol. 13, no. 12, p. 5484, 1976.

[4] M. Poelker, P. Adderley, J. Brittian, J. Clark, J. Grames, J. Hansknecht, J. McCarter, M. Stutzman, R. Suleiman, and K. Surles-Law, "High intensity polarized electron sources," in *AIP Conference Proceedings*, vol. 980, pp. 73–78, 2008.

[5] M. Hayashi, "Recommended values of transport cross sections for elastic collisions and total cross section for electrons in atomic and molecular gases," *Inst. Plasma Phys., Nagoya University, Report IPPJ-AM-19 (Nov. 1981)*, 1981.

[6] M. Alguard, J. Clendenin, R. Ehrlich, V. Hughes, J. Ladish, M. Lubell, K. Schüler, G. Baum, W. Raith, R. H. Miller, *et al.*, "A source of highly polarized electrons at the stanford linear accelerator center," *Nuclear Instruments and Methods*, vol. 163, no. 1, pp. 29–59, 1979.

[7] W. von Drachenfels, U. Koch, T. M. Müller, W. Paul, and H. Schaefer, "A pulsed source for polarized electrons with high repetition rate," *Nuclear Instruments and Methods*, vol. 140, no. 1, pp. 47–55, 1977.

[8] R. L. Bell, *Negative electron affinity devices*. Oxford University Press, 1973.

[9] G. Lampel and C. Weisbuch, "Proposal for an efficient source of polarized photoelectrons from semiconductors," *Solid State Communications*, vol. 16, no. 7, pp. 877–880, 1975.

[10] D. Pierce, F. Meier, and P. Zürcher, "Direct observation of spin dependent electronic structure of gaas using spin polarized photoemission," *Physics Letters A*, vol. 51, no. 8, pp. 465–466, 1975.

[11] J. Scheer and J. Van Laar, "Gaas-cs: A new type of photoemitter," *Solid State Communications*, vol. 3, no. 8, pp. 189–193, 1965.

[12] T. Nakanishi, H. Aoyagi, H. Horinaka, Y. Kamiya, T. Kato, S. Nakamura, T. Saka, and M. Tsubata, "Large enhancement of spin polarization observed by photoelectrons from a strained gaas layer," *Physics Letters A*, vol. 158, no. 6, pp. 345–349, 1991.

[13] T. Omori, Y. Kurihara, T. Nakanishi, H. Aoyagi, T. Baba, T. Furuya, K. Itoga, M. Mizuta, S. Nakamura, Y. Takeuchi, *et al.*, "Large enhancement of polarization observed by extracted electrons from the algaas-gaas superlattice," *Physical review letters*, vol. 67, no. 23, p. 3294, 1991.

[14] K. Aulenbacher, "Polarized beams for electron accelerators," *The European Physical Journal Special Topics*, vol. 198, no. 1, pp. 361–380, 2011.

[15] J. Grames, R. Suleiman, P. Adderley, J. Clark, J. Hansknecht, D. Machie, M. Poelker, and M. Stutzman, "Charge and fluence lifetime measurements of a dc high voltage gaas photogun at high average current," *Physical Review Special Topics-Accelerators and Beams*, vol. 14, no. 4, p. 043501, 2011.

[16] C. Sinclair, P. Adderley, B. Dunham, J. Hansknecht, P. Hartmann, M. Poelker, J. Price, P. Rutt, W. Schneider, and M. Steigerwald, "Development of a high average current polarized electron source with long cathode operational lifetime," *Physical Review Special Topics-Accelerators and Beams*, vol. 10, no. 2, p. 023501, 2007.

[17] C. K. Sinclair, "Recent advances in polarized electron sources," in *Particle Accelerator Conference, 1999. Proceedings of the 1999*, vol. 1, pp. 65–69, IEEE, 1999.

[18] K. Aulenbacher *et al.*, "Contribution to the workshop on photocathodes of polarized sources for accelerators," *SLAC-432*, 1994.

[19] A. Accardi *et al.*, "Electron ion collider: The next qcd frontier," *arXiv preprint arXiv:1212.1701*.

[20] A. Deshpande, "Electron ion collider: The next qcd frontier," in *APS Meeting Abstracts*, vol. 1, 2013.

[21] V. Ptitsyn, E. Aschenauer, J. Beebe-Wang, S. Belomestnykh, I. Ben-Zvi, R. Calaga, X. Chang, A. Fedotov, H. Hahn, L. Hammons, *et al.*, "High luminosity electron-hadron collider erhic," in *Particle Accelerator Conference, 2011. Proceedings of IPAC'11*, 2011.

[22] P. Adderley, J. Clark, J. Grames, J. Hansknecht, M. Poelker, M. Stutzman, R. Suleiman, K. Surles-Law, J. McCarter, and M. BastaniNejad, "Cebaf 200kv inverted electron gun,"

[23] E. Tsentalovich, "Status of high intensity polarized electron gun project," in *Proceedings of the XVth International Workshop on Polarized Sources, Targets, and Polarimetry (PSTP2013). 9-13 September, 2013. Charlottesville, Virginia, USA. Online at http://pos. sissa. it/cgi-bin/reader/conf. cgi? confid= 182, id. 43*, vol. 1, p. 43, 2013.

[24] V. Litvinenko, "Gatling gun: high average polarized current injector for erhic," tech. rep., Brookhaven National Laboratory (BNL) Relativistic Heavy Ion Collider, 2010.

[25] D. Young, "Proceedings of the heavy ion fusion workshop held at brookhaven national laboratory, upton, new york, 17 october 1977," tech. rep.

[26] J. Stovall, F. Guy, R. Stokes, and T. Wangler, "Beam funneling studies at los alamos," *Nuclear Instruments and Methods in Physics Research Section A: Accelerators, Spectrometers, Detectors and Associated Equipment*, vol. 278, no. 1, pp. 143–147, 1989.

[27] C. W. Leemann, D. R. Douglas, and G. A. Krafft, "The continuous electron beam accelerator facility: Cebaf at the jefferson laboratory," *Annual Review of Nuclear and Particle Science*, vol. 51, no. 1, pp. 413–450, 2001.

[28] K. Aulenbacher, V. Tioukine, M. Wiessner, and K. Winkler, "Status of the polarized source at mami," in *AIP CONFERENCE PROCEEDINGS*, pp. 1088–1092, IOP INSTITUTE OF PHYSICS PUBLISHING LTD, 2003.

[29] W. E. Spicer and A. Herrera-Gomez, "Modern theory and applications of photocathodes," in *SPIE's 1993 International Symposium on Optics, Imaging, and Instrumentation*, pp. 18–35, International Society for Optics and Photonics, 1993.

[30] W. Spicer, "Negative affinity 3–5 photocathodes: Their physics and technology," *Applied physics*, vol. 12, no. 2, pp. 115–130, 1977.

[31] P. J. Sáez, *Polarization and charge limit studies of strained GaAs photocathodes*. PhD thesis, Stanford University, 1997.

[32] L. James, G. Antypas, J. Edgecumbe, R. Moon, and R. Bell, "Dependence on crystalline face of the band bending in cs2 o-activated gaas," *Journal of Applied Physics*, vol. 42, no. 12, pp. 4976–4980, 1971.

[33] C. Kittel, *Introduction to solid state physics*. Wiley, 2005.

[34] W. Spicer, "Photoemissive, photoconductive, and optical absorption studies of alkali-antimony compounds," *Physical review*, vol. 112, no. 1, p. 114, 1958.

[35] A. L. Hughes and L. A. DuBridge, *Photoelectric phenomena*, vol. 119. McGraw Hill book company, inc., 1932.

[36] R. Broudy, V. Mazurczyk, R. Willardson, and A. Beer, "Semiconductors and semimetals," *Academic, New York*, vol. 157, 1981.

[37] E. Wang, *High quantum efficiency photocathode for use in superconducting RF gun*. PhD thesis, School of Physics, Peking University, 2012.

[38] D. Pierce, F. Meier, and P. Zürcher, "Negative electron affinity gaas: A new source of spin-polarized electrons," *Applied Physics Letters*, vol. 26, no. 12, pp. 670–672, 1975.

[39] D. Pierce, R. Celotta, G.-C. Wang, W. Unertl, A. Galejs, C. Kuyatt, and S. Mielczarek, "The gaas spin polarized electron source," *Review of Scientific Instruments*, vol. 51, no. 4, pp. 478–499, 1980.

[40] A. Aleksandrov, N. Dikansky, R. Gromov, and P. Logatchov, "Experimental study of gaas photocathode performance in rf gun," in *Particle Accelerator Conference, 1999. Proceedings of the 1999*, vol. 1, pp. 78–80, IEEE, 1999.

[41] J. Kewischa, I. Ben-Zvi, T. Rao, A. Burrill, D. Pate, E. Wang, R. Todd, H. Bluem, D. Holmes, and T. Schultheiss, "The polarized srf gun experiment," in *Workshop on Polarized Electron Sources and Polarimeters*, p. 1133, Citeseer, 2008.

[42] D. Rodway and M. Allenson, "In situ surface study of the activating layer on gaas (cs, o) photocathodes," *Journal of Physics D: Applied Physics*, vol. 19, no. 7, p. 1353, 1986.

[43] T. Wada, T. Nitta, T. Nomura, M. Miyao, and M. Hagino, "Influence of exposure to co, co2 and h2o on the stability of gaas photocathodes," *Japanese journal of applied physics*, vol. 29, no. 10R, p. 2087, 1990.

[44] M. Miyao, T. Wada, T. Nitta, and M. Hagino, "The state of cs on negative electron affinity surfaces," *Applied Surface Science*, vol. 33, pp. 364–369, 1988.

[45] K. Aulenbacher, C. Nachtigall, H. Andresen, J. Bermuth, T. Dombo, P. Drescher, H. Euteneuer, H. Fischer, D. Harrach, P. Hartmann, *et al.*, "The mami source of polarized electrons," *Nuclear Instruments and Methods in Physics Research Section A: Accelerators, Spectrometers, Detectors and Associated Equipment*, vol. 391, no. 3, pp. 498–506, 1997.

[46] M. Reiser, *Theory and design of charged particle beams*. John Wiley & Sons, 2008.

[47] X. Chang, I. Ben-Zvi, J. Kewisch, V. Litvinenko, A. Pikin, V. Ptitsyn, T. Rao, B. Sheehy, J. Skaritka, E. Wang, *et al.*, "A multiple cathode gun design for the erhic polarized electron source," in *Proceedings of PAC*, p. 1969, 2011.

[48] X. Chang, I. Ben-Zvi, J. Kewisch, V. Litvinenko, W. Meng, A. Pikin, V. Ptitsyn, T. Rao, B. Sheehy, J. Skarita, *et al.*, "Rotating dipole and quadrupole field for a multiple cathode system," tech. rep., Brookhaven National Laboratory (BNL) Relativistic Heavy Ion Collider, 2011.

[49] E. Wang, I. Ben-Zvi, D. Gassner, W. Meng, T. Rao, E. Riehn, J. Skaritka, and O. Rahman, "Beam dynamics of funneling multiple bunches electrons," *TUPSM08, NA-PAC*, vol. 13, 2013.

[50] I. Ben-Zvi, X. Chang, V. Litvinenko, W. Meng, A. Pikin, and J. Skaritka, "Generating high-frequency, rotating magnetic fields with low harmonic content," *Physical Review Special Topics-Accelerators and Beams*, vol. 14, no. 9, p. 092001, 2011.

[51] M. Bastaninejad, A. Elmustafa, E. Forman, J. Clark, S. Covert, J. Grames, J. Hansknecht, C. Hernandez-Garcia, M. Poelker, and R. Suleiman, "Improving the performance of stainless-steel dc high voltage photoelectron gun cathode electrodes via gas conditioning with helium or krypton," *Nuclear Instruments and Methods in Physics Research Section A: Accelerators, Spectrometers, Detectors and Associated Equipment*, vol. 762, pp. 135–141, 2014.

[52] D. Faircloth, "Technological aspects: High voltage," *arXiv preprint arXiv:1404.0952*, 2014.

[53] R. Kersevan and J.-L. Pons, "Introduction to molflow+: New graphical processing unit-based monte carlo code for simulating molecular flows and for calculating angular coefficients in the compute unified device architecture environment," *Journal of Vacuum Science & Technology A*, vol. 27, no. 4, pp. 1017–1023, 2009.

[54] "ULVAC AxTRAN gauge reference manual." `http://www.ulvac.com/userfiles/files/Vacuum%20Gauges/Extremely%20High%20vacuum%20gauge%20AxTRAN.pdf`.

[55] H. Tawara, Y. Itikawa, H. Nishimura, and M. Yoshino, "Cross sections and related data for electron collisions with hydrogen molecules and molecular ions," *Journal of Physical and Chemical Reference Data*, vol. 19, no. 3, pp. 617–636, 1990.

[56] O. Malyshev, A. Smith, R. Valizadeh, and A. Hannah, "Electron stimulated desorption from bare and nonevaporable getter coated stainless steels," *Journal of Vacuum Science & Technology A*, vol. 28, no. 5, pp. 1215–1225, 2010.

[57] O. L. Vacuum, "Fundamentals of vacuum technology," 2007.